Ore Geology Reviews 126 (2020) 103717

Contents lists available at ScienceDirect

Ore Geology Reviews

journal homepage: www.elsevier.com/locate/oregeorev

Petrogenesis of Early Cretaceous adakites in Tongguanshan Cu–Au polymetallic deposit, Tongling region, Eastern China

Xiao-Yan Jiang[a,*], Jiang-Hong Deng[b,c], Jin-Cheng Luo[a], Li-Peng Zhang[b,c,*], Ze-Bin Luo[d,e], Hai-Bo Yan[d,e], Wei-Dong Sun[b,c,d]

[a] State Key Laboratory of Ore Deposit Geochemistry, Institute of Geochemistry, Chinese Academy of Sciences, Guiyang 550081, China
[b] Laboratory for Marine Mineral Resources, Pilot National Laboratory for Marine Science and Technology (Qingdao), Qingdao 266237, China
[c] Center of Deep Sea Research, Center of Ocean Mega-Science, Institute of Oceanology, Chinese Academy of Sciences, Qingdao 266071, China
[d] University of Chinese Academy of Sciences, Beijing 100049, China
[e] CAS Key Laboratory of Mineralogy and Metallogeny, Guangzhou Institute of Geochemistry, Chinese Academy of Sciences, Guangzhou 510640, China

ARTICLE INFO

Keywords:
Adakite
Geochemistry
Cu-Au mineralization
Tongguanshan deposit
Tongling

ABSTRACT

Adakites are closely related to Cu–Au deposits in many regions worldwide. The petrogenesis of the Early Cretaceous adakites in the Lower Yangtze River Belt (LYRB) of East China and their genetic relationship with Cu-Au polymetallic mineralization are still debated. The Tongguanshan (TGS) pluton is representative of the adakitic intrusions in the Tongling region and is composed of granodiorite and quartz monzodiorite, and contains quartz monzodiorite enclaves. Zircons from the granodiorite yield a SIMS U-Pb crystallization age of 136.7 ± 1.4 Ma, which suggests that the Cretaceous magmatism is related to the mineralization. The host rocks and enclaves have SiO_2 contents of 61.2–65.3 wt% and 54.9–58.0 wt%, respectively. Both the host rocks and the enclaves are characterized by high Al_2O_3 and Sr, and low Y and Yb contents, as well as high Sr/Y and $(La/Yb)_N$ ratios, which are typical geochemical characteristics of adakites, and they can be further divided into high-silica (host rock) and low-silica (enclave) adakites. The large range of $\varepsilon_{Hf}(t)$ and $\delta^{18}O$ values of the host rocks (−11.6 to − 21.9, 6.8‰–7.6‰, respectively) and of the enclaves (−13.8 to − 23.6, 6.9‰–7.3‰, respectively), suggest an enriched and heterogeneous source. The host rocks and enclaves have similar Sr-Nd isotopic compositions ($\varepsilon_{Nd}(t)$ = −9.73 to −11.4, I_{Sr} = 0.7068 to 0.7073), which are intermediate among those of MORB, marine sediment, and the Yangtze lower crust. Whole-rock element ratios suggest that the host rocks were generated by the partial melting of subducted oceanic crust mixed with sediments, followed by assimilation of the lower crust. In contrast, the enclaves were derived from partial melting of enriched mantle metasomatized by slab-derived melts. Magma mixing, crustal contamination, and metasomatism play roles in generating the geochemical variations in the TGS adakites. The high oxygen fugacity and high contents of slab-derived volatiles suggested by apatites are favorable for large-scale Cu mineralization in the Tongling area, LYRB.

1. Introduction

The term 'adakite' was first proposed to describe intermediate to felsic igneous rocks that were produced by partial melting of subducted hot, young oceanic crust (Defant and Drummond, 1990). These rocks have distinctively geochemical characteristics, including SiO_2 contents of ≥56 wt%, Al_2O_3 contents of ≥15 wt%, high Sr contents (mostly ≥ 400 ppm) and Sr/Y (≥20) ratios, low Y and Yb contents (generally ≤ 18 ppm and ≤ 1.9 ppm, respectively), and the absence of Eu anomalies (Drummond and Defant, 1990; Martin, 1999). It has recently been shown that, in addition to slab melting (Drummond and Defant, 1990; Martin, 1999; Moyen, 2009; Zhang et al., 2017; Deng et al., 2019, 2020; Hernández-Uribe et al., 2020), adakitic magmas can be generated by other mechanisms in different tectonic environments, including partial melting of thickened lower continental crust by basaltic underplating or delamination (Petford and Atherton, 1996; Guo et al., 2007; Goss and Kay, 2009; He et al., 2011; Li et al., 2019), fractionation from hydrous basalts (Castillo et al., 1999; Richards and Kerrich, 2007; Ma et al., 2015), and interaction between slab-derived melt and mantle peridotite (Bourdon et al., 2002; Wang et al., 2008). Because there is a genetic link between the adakites and a majority of known Cu–Au mineralization, the generation of adakites has attracted

* Corresponding authors at: State Key Laboratory of Ore Deposit Geochemistry, Institute of Geochemistry, Chinese Academy of Sciences, Guiyang 550081, China (X.-Y. Jiang).
E-mail addresses: jiangxiaoyan@mail.gyig.ac.cn (X.-Y. Jiang), zhanglipeng@qdio.ac.cn (L.-P. Zhang).

https://doi.org/10.1016/j.oregeorev.2020.103717
Received 5 March 2020; Received in revised form 31 July 2020; Accepted 8 August 2020
Available online 14 August 2020
0169-1368/

widespread attention (e.g. Thiéblemont et al., 1997; Borisova et al., 2006; Sillitoe, 2010; Sun et al., 2010a, 2010b, 2011, 2012, 2015, 2017; Deng et al., 2016, 2019, 2020; Zhang et al., 2017; Hernández-Uribe et al., 2020).

Accessory minerals reflect the geochemical characteristics of their host rocks and place constraints on their petrogenesis and magmatic processes that may not be apparent using whole-rock chemistry (Miles et al., 2013; Bruand et al., 2014a, 2014b; Duan et al., 2019). Zircon is a common robust accessory mineral in magmatic rocks, which incorporates a variety of trace elements and preserves the isotopic composition of its parent magma, used to investigate crystallization age and trace petrogenesis (Hoskin and Ireland, 2000; Hoskin and Schaltegger, 2003; Hawkesworth and Kemp, 2006; Kemp et al., 2007; Gagnevin et al., 2010). Apatite is another important accessory mineral, which buffers trace element compositions and most of the halogen contents. Apatite displays great potential in metallogenic studies (Barth et al., 2013; Bouzari et al., 2016; Mao et al., 2016; Pan et al., 2016), especially in evaluating the physiochemical conditions of ore-forming processes and placing constraints on magmatic processes (Boyce and Hervig, 2009; Patiño Douce et al., 2011; Bruand et al., 2014; Harlov, 2015; Kusebauch et al., 2015; Jiang et al., 2018a,b).

The Lower Yangtze River Belt (LYRB) hosts abundant Mesozoic magmatic rocks and economic mineral deposits. Studies reveal that Cu-Au ore deposits in the LYRB are both spatially and temporally associated with Early Cretaceous adakites (Li et al., 2013; Wu et al., 2017; Xie et al., 2017; Du et al., 2018; Gu et al., 2020; Wang et al., 2020). However, the genesis of those adakites remains controversial, and several different models have been proposed: (1) partial melting of subducted oceanic crust, mixing with metasomatized mantle-derived magmas and old crustal components (Ling et al., 2009; Xie et al., 2017, 2019; Hu et al., 2018); (2) fractional crystallization of basaltic magma possibly coupled with crustal contamination (Li et al., 2009a,b; Du et al., 2018); (3) derived from delaminated lower continental crust (LCC), interaction with the mantle peridotites (Wang et al., 2004, Wang et al., 2006, Wang et al., 2007); (4) originated from enriched mantle source, metasomatized by dewatering from a delaminated-slab (Li et al., 2013), or mixed by crustal melts (Yan et al., 2015). Analogously, the large-scale Cu-Au metallogenesis is also controversial, genetically related to the delaminated LCC (Wang et al., 2004) or the subducted oceanic slab (Xie et al., 2017, 2018).

The Tongling metallogenic region of Anhui Province is an important polymetallic ore district in the LYRB (Fig. 1; Chang et al., 1991; Zhai et al., 1996; Pan and Dong, 1999). The formation of the Cu-Au polymetallic deposits in this region is closely related to Late Mesozoic intrusions (Wang et al., 2003; Xie et al., 2009; Mao et al., 2011; Yang et al., 2014; Wang et al., 2016; Xie et al., 2012, 2017). However, the petrogenesis still need to be further clarified. The Mesozoic adakites in Tongguanshan (TGS) are tightly associated with the Cu-Au ore deposits in the Tongling region, LYRB. In this study, we integrated an analysis of mineral chemistry of zircon and apatite, combined with systematical analyses of whole-rock geochemistry of the corresponding adakites. It is aimed to provide firm constraints on the petrogenesis of the adakitic rocks and the associated Cu-Au metallogenesis through the integrated study of accessory minerals and whole-rock geochemistry.

2. Geological background and sample descriptions

The LYRB is located on the northern margin of the Yangtze Block, separated from the Jiangnan domain to the southeastern by Yangxing-Changzhou fault, and from the North China Craton and Dabie Orogenic Belt to the northwestern by the NW-trending Xiangfan-Guangji and Tan-Lu faults (Fig. 1). The oldest basement in the Yangtze Craton are the > 3.2 Ga Kongling Group gneisses (Guo et al., 2014), which are overlain by ~ 2000 m thick Paleoproterozoic–Neoproterozoic (1850–990 Ma) volcano-sedimentary succession (Pan and Dong, 1999). That succession is unconformably overlain by voluminous Neoproterozoic bimodal volcanic rocks (825–740 Ma), represented in south Anhui by the Shangxi Group and Jingtan Formation (Wang et al., 2013a, 2013b; Zhang and Zheng, 2013). Above these lie Cambrian mudstones and argillaceous limestones containing chert nodules, Ordovician limestones and dolomitic limestones, Silurian clastic rocks, Devonian sandstones, Carboniferous sandstones, siltstones and limestones, Permian shales and limestones, and Triassic argillaceous clastic rocks (Chang et al., 1991; Zhai et al., 1992). Extensive Late Mesozoic magmatic rocks were intruded into the Neoproterozoic low-grade metamorphic rocks and the Paleozoic to Triassic sedimentary strata.

Tongling is located in the Yangtze craton in central eastern China (Fig. 1). Marine deposits in Tongling include Carboniferous carbonate, Permian limestone and black shale, and Triassic carbonate and argillaceous rocks, with the exception of the Middle–Late Devonian. Mesozoic volcano–sedimentary basins, are widely distributed above these marine deposits (Fig. 2; Chang et al., 1991; Wang et al., 2000; Wang et al., 2013a, 2013b). A series of NE-trending folds and faults impact the shapes of the Late Mesozoic magmatic rocks (comprising > 70 intrusions). These intrusions are widely distributed along the EW-trending Tongling–Nanling Fault and intruded into the Silurian–Triassic sedimentary sequences. Intermediate–felsic intrusions and associated hydrothermal activity produced numerous polymetallic Cu–Au deposits, which form a ~ 40 × 20 km tectonic–magmatic–mineralization zone (Fig. 1; Zhai et al., 1992). Plutons with ore deposits include the TGS, Shizishan, Dongguashan, Xinqiao, and Fenghuangshan plutons, which are composed mainly of pyroxene monzodiorite, quartz monzodiorite, and granodiorite (closely related to Cu polymetallic deposits) (Chen et al., 2016; Xie et al., 2017).

The TGS copper field is typical of the skarn-type orefields in the LYRB (Tian et al., 2005). It is located in the west of EW-trending Tongling–Daijiahui basement fault and the northwest of the TGS 'S' shaped anticline (Cui et al., 2002). A series of NE-, NNE-, NW- and NNW- trending faults had multiple stages of movement, and are closely associated with the intrusions and ore formation (Xu et al., 2019). The exposed strata are mainly Silurian–Triassic marine clastic sediments and carbonates, which have a thickness of 3–4 km (Tian et al., 2005). The TGS ore deposit is composed of eight blocks, including the Songshushan and Xiaotongguanshan blocks (Fig. 2). The ore minerals are mainly chalcopyrite, magnetite, pyrrhotite and pyrite, with minor bornite, chalcocite, tetrahedrite, sphalerite, and molybdenite. The gangue minerals include quartz, calcite, garnet, diopside, and talc (Xu et al., 2019).

The TGS pluton is a NE–SW-trending intermediate-to-shallow rock, which has an elliptical shape and crops out over an area of ~ 2 km^2 (Figs. 1 and 2). The pluton intruded into Carboniferous and Permian strata, and was emplaced near the axis of an anticline. Sixteen fresh representative samples of TGS granodiorite and quartz monzodiorite were collected (Fig. 2). The samples are light to dark grey, coarse- to medium-grained, massive (Fig. 3a and b), and composed of plagioclase (60%–65%), quartz (13%–20%), amphibole (10%–15%), K-feldspar (~5%), biotite (1%–5%), and minor zircon, apatite, titanite and Fe–Ti oxides (Fig. 3c and d). Microgranular enclaves are distributed in the east of the pluton, of which four samples were collected. Most of the enclaves are round or globular and several to tens of centimeters in diameter (Fig. 3a and b). They are quartz monzodiorite, dark in color, fine-grained, and some have back- veins (Fig. 3b). They are composed of plagioclase, K-feldspar, amphibole and quartz (Fig. 3e), and have more mafic minerals and plagioclase and less quartz than the host rocks. The apatites in the enclaves are all acicular.

3. Analytical methods

3.1. SIMS zircon U–Pb dating

Zircon was separated from sample TGS15 (quartz monzodiorite) using standard density and magnetic separation techniques.

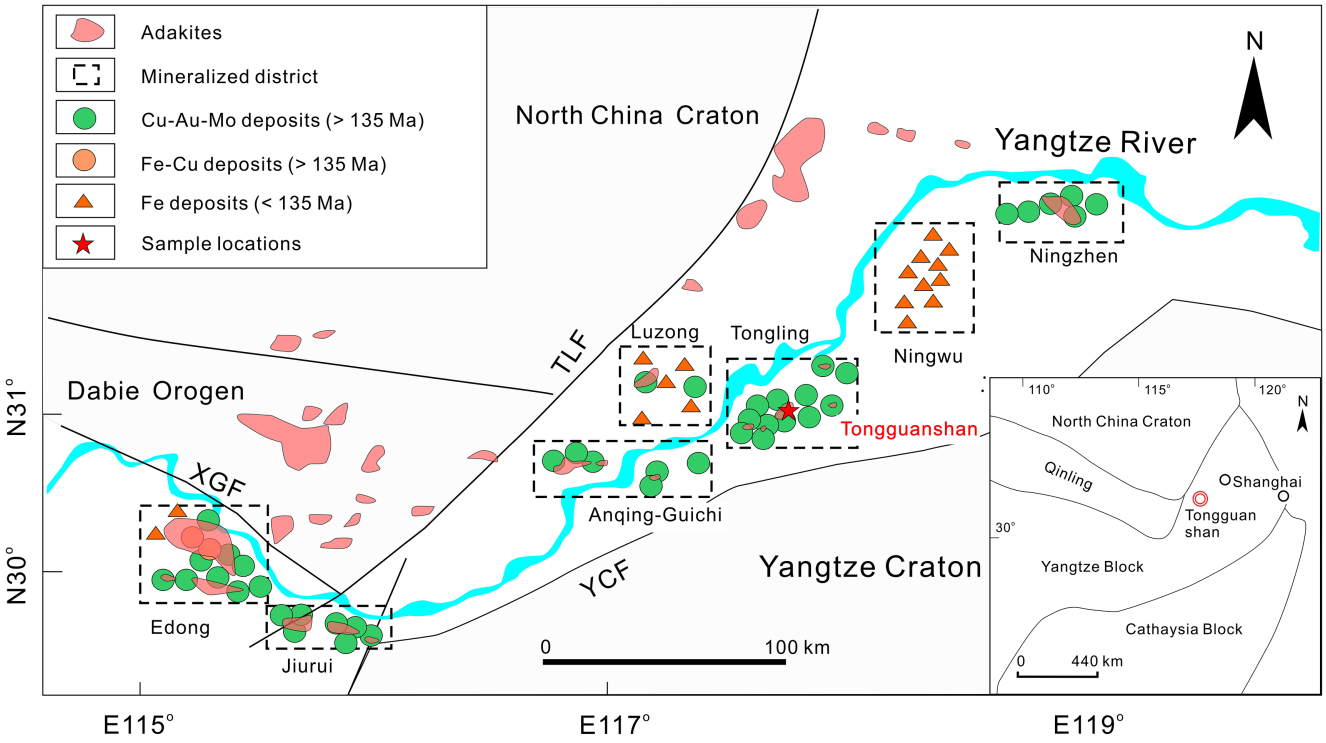

Fig. 1. Geological sketch map of the distribution of adakites and ore deposits along Yangtze River, modified after Pan and Dong (1999) and Deng et al. (2016). Tectonic sketch map of eastern China in the inner part. XGF – Xiangfan–Guangji Fault; TLF – Tancheng–Lujiang Fault; YCF – Yangxin–Changzhou Fault.

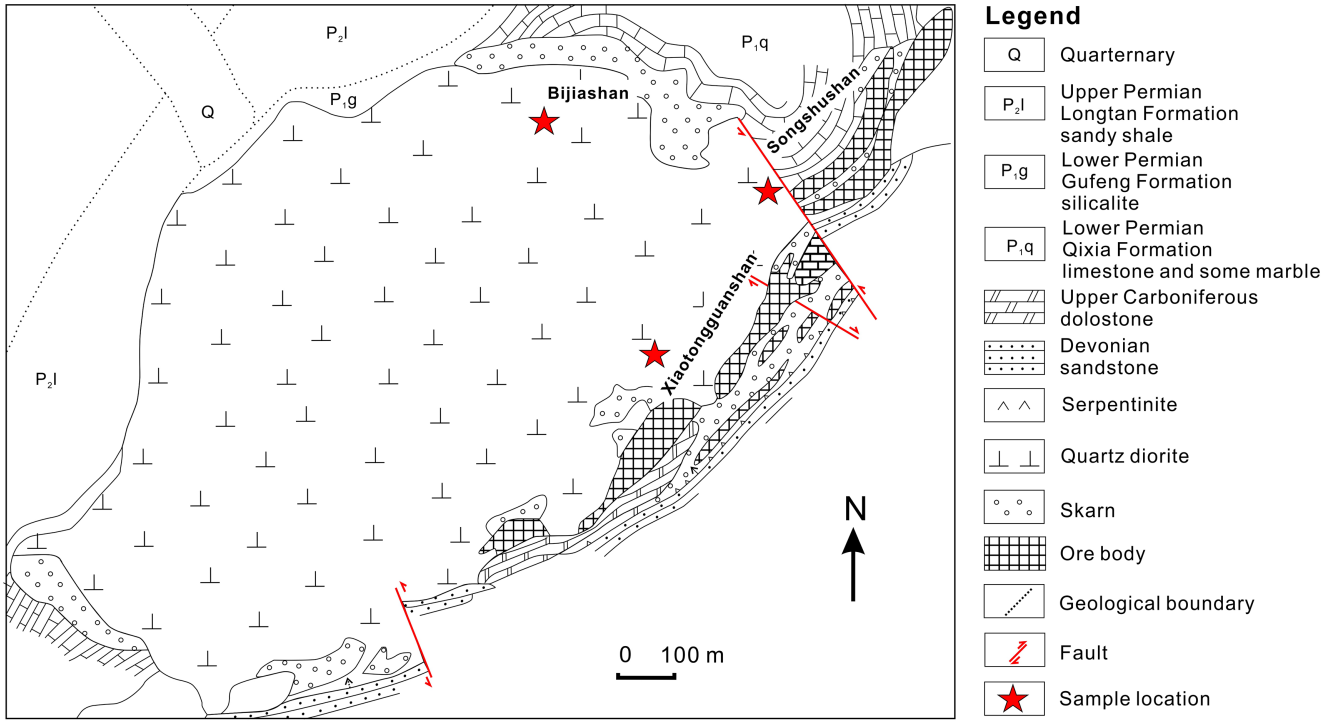

Fig. 2. Geological map of the Tongguanshan Cu-Au deposit (after Cui et al., 2002; Xu et al., 2004).

Approximately 200 zircon grains from the sample, were mounted with zircon standards in epoxy mount. The mount was then polished to expose the inside of the zircon grains. Transmitted and reflected light microphotographs and cathodoluminescence (CL) images were taken to reveal their internal structure. Prior to SIMS analysis, the mount was vacuum-coated with high-purity gold.

Zircon U–Pb isotopic compositions were analyzed on a CAMECA IMS 1280HR at the Guangzhou Institute of Geochemistry, Chinese Academy of Sciences (GIGCAS), using standard operating conditions (7-scan cycle, ~8nA primary O^{2-} beam, 20 × 30 μm spot size, and a mass resolving power of ~ 5400). U–Pb ratios were determined relative to the Plešovice standard zircon ($^{206}Pb/^{238}U$ = 0.05369; 337.1 Ma; Sláma et al., 2008), and the absolute abundances were determined relative to the M257 standard zircon (U = 840 ppm, Th/U = 0.27; Nasdala et al.,

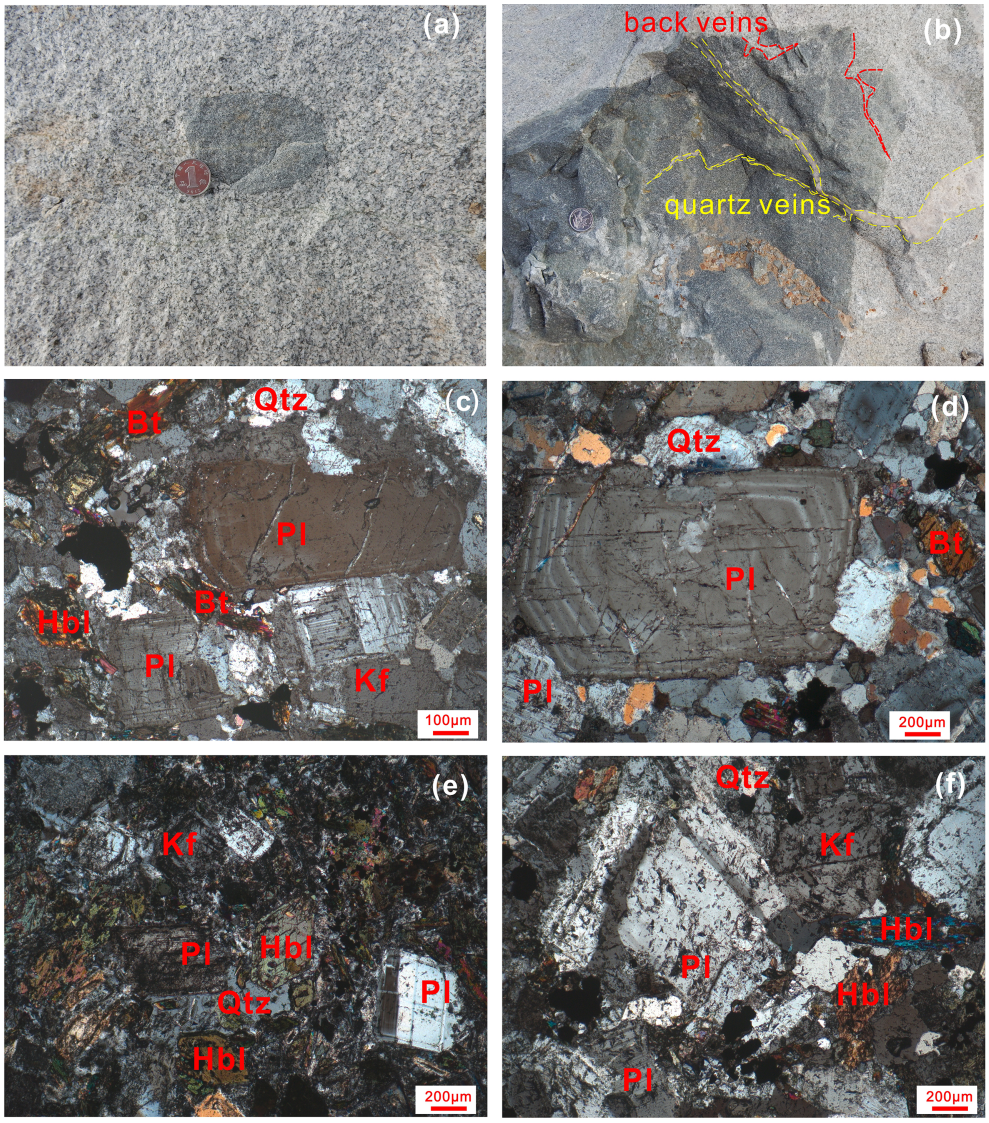

Fig. 3. Field and photomicrographs illustrating fabric and minerals of the rocks in the Tongguanshan pluton. (a) Field photograph of granodiorite (sample TGS01), (b) Field photograph of quartz monzodiorite (sample TGS10); (c) thin section photograph of granodiorite (sample TGS01, cross-polarized light); (d) photomicrograph of quartz monzodiorite (sample TGS05, cross-polarized light), (e) thin section photograph of quartz monzodiorite (sample TGS10, cross-polarized light); (f) photomicrograph of quartz monzodiorite (sample TGS 15, cross-polarized light). Abbreviations in the images: Pl, plagioclase; Kfs, potassic feldspar; Hbl, hornblende; Bi, biotite; Qtz, quartz.

2008). The Plešovice zircon was analyzed periodically between each group of five analyses. Operating and data processing procedures followed those of Li et al. (2009). Common Pb was corrected using ^{204}Pb. Uncertainties on individual analyses are reported at the 1σ level, and mean ages for pooled U–Pb analyses are quoted with 95% confidence intervals. Data reduction was carried out using Isoplot/Exv. 3.70 (Ludwig, 2008). To monitor the accuracy of SIMS U–Pb measurements, the in-house Qinghu zircon standard was periodically analyzed, eight analyses of which yield a concordant age of 158.1 ± 1.7 Ma (MSWD = 0.34), within error of the reported age (159.5 ± 0.2 Ma; Li et al., 2013). SIMS zircon U–Pb age data are listed in Supplementary material Table S1.

3.2. Whole-rock major and trace elements

Twenty fresh samples were crushed and ground to 200 mesh particle size. A representative aliquot of the powder for each sample was dried at 105 °C for 4 h prior to analyze on an X-ray fluorescence spectrometer at the ALS Laboratory Group. Analytical chemistry and testing services (Guangzhou) in the form of fused glass beads. Precision for the analytical results is typically 1–5%. An Agilent 7700e ICP-MS (inductively coupled plasma mass spectrometry) was used for conducting whole-rock trace element analyses at the Wuhan SampleSolution Analytical Technology Co., Ltd., Wuhan, China. The detailed sample-digesting procedure for ICP-MS analyses and analytical precision and accuracy are identical to those of Liu et al. (2008). The signal drift of the spectrometer was monitored by an internal standard Rh solution, whereas element concentrations of unknown were calibrated using concurrently treated standards. Standards chosen include AGV-2, BHVO-2, BCR-2 and RGM-2. The precision during trace element analysis for most elements was generally better than 5%. Major and trace elements are listed in Supplementary material Table S2.

3.3. In situ SIMS zircon oxygen isotopes

Zircons of TGS15 (host rock) and TGS10 (enclave) were measured oxygen isotopes using the same CAMECA IMS 1280HR at laboratory in GIGCAS. Before SIMS oxygen isotope analysis, the sample mount was reground to ensure that any oxygen implanted in the zircon surface from the O_2^- beam used for U-Pb analysis was removed. The Cs^+ ion beam was accelerated to 10 kV, with an intensity of ~ 2nA, focused to a ~ 20 μm spot. Oxygen isotopes were measured in multi-collector mode with two off-axis Faraday cups. The normal incidence electron flood gun was used to compensate for sample charging. The NMR (nuclear magnetic resonance) was used for stabilizing magnetic field. Detailed analytical procedures are in the same way as described by Li et al. (2010a). The instrumental mass fractionation factor (IMF) was corrected using Penglai zircon standard, which has a $\delta^{18}O$ value of

5.31‰ (Li et al., 2010b). The internal precision of a single analysis was generally better than 0.2‰ (1σ standard error) for $^{18}O/^{16}O$ ratio. The external precision, measured by the reproducibility of repeated analyses of Penglai standard during this study, is 0.42‰ (2SD, n = 13). During the course of this study, an in-house zircon standard Qinghu was also measured between unknowns. Twenty-seven measurements of Qinghu zircon yield a weighted mean of $\delta^{18}O = 5.35 \pm 0.50‰$ (2SD), consistent within errors with the reported value of 5.4 ± 0.2‰ (Li et al., 2013). In situ O isotopic results are listed in Supplementary material Table S3.

3.4. LA-MC-ICPMS zircon Lu-Hf analyses

In situ zircon Lu-Hf isotopic measurements (same samples as oxygen analysis) were performed on a Neptune Plus MC-ICP-MS, coupled with a 193 nm laser ablation system at the State Key Laboratory of Continental Dynamics, Northwest University, Xi'an, China. The detail information of these instruments can be found in Bao et al. (2017), and the analysis strategy and calibration method are similar to those described by Yuan et al. (2008). LA-MC-ICPMS zircon Hf-isotope was analyzed following the SIMS U-Pb and O isotopic isotope measurement. This sequence of measurements enables U-Pb age and Hf-O isotopic compositions to be done on the sites shown in Fig. 4. The laser beam diameter is 44 μm with the repetition rate of 10 Hz. The standard zircons 91,500 and MudTank during the course of this study yielded a weighted mean of $^{176}Hf/^{177}Hf = 0.282304 \pm 0.000036$ (N = 11, 2σ) and 0.282496 ± 0.000029 (N = 6, 2σ), which are in good agreement within errors with the reported value (0.282311 ± 0.000007, 2σ; 0.282520 ± 0.000016, 2σ) (Yuan et al., 2008). Zircon Lu-Hf isotope ratios and $\varepsilon_{Hf}(t)$ values are presented in Supplementary material Table S3.

3.5. Whole-rock Sr-Nd isotopic analyses

Three samples, including TGS05 and TGS15 (host rock) and TGS10 (enclave), were chosen for whole-rock Sr-Nd isotope analysis. Strontium and Nd isotopic compositions were performed on a Micromass Isoprobe multi-collector–ICP–MS (MC–ICP–MS) at the State Key Laboratory of Isotope Geochemistry, GIGCAS. ~ 100 mg samples were dissolved in HF + HNO_3 acid in Teflon bombs at ~ 195 °C for two days. Strontium and rare earth elements (REE) were separated using cation-exchange resin; Nd fractions were further separated by HDEHP-coated Kef columns. Detailed chemical procedures are similar to those described by Li et al. (2004). The MC–ICP–MS was operated in static mode and analyses of the NBS SRM 987 and Shin Etsu JNdi-1 standards yielded $^{87}Sr/^{86}Sr$ and $^{143}Nd/^{144}Nd$ values of 0.710242 ± 10 (2σ, n = 9) and 0.512115 ± 10 (2σ, n = 8), respectively. Measured Sr and Nd isotope ratios were normalized to $^{86}Sr/^{88}Sr = 0.1194$ and $^{146}Nd/^{144}Nd = 0.7219$ using the exponential law. Analyses of the NBS SRM 987 and Shin Etsu JNdi-1 standards yielded $^{87}Sr/^{86}Sr$ and $^{143}Nd/^{144}Nd$ ratios that were within error of the recommended values of $^{87}Sr/^{86}Sr = 0.71025$ and $^{143}Nd/^{144}Nd = 0.512115$, respectively (Tanaka et al., 2000). The whole-rock Sr and Nd isotopic data are given in Supplementary material Table S4.

3.6. Apatite major and trace elements analyses

Apatite crystals from the host rock (TGS01) and an enclave (TGS10) were separated and mounted in epoxy then polished to expose a cross section for analysis. CL images were taken before electron microprobe and LA–ICP–MS analyses.

Major elements compositions of the apatite were analyzed using of wavelength-dispersive spectrometers (WDS) on a JEOL JXA-8230 electron microprobe at the Testing Center of the Shandong office of the China Metallurgical Geology Bureau, Jinan, China. The analyses used an accelerating voltage of 15 kV, a beam current of 10nA, and a defocused beam 10 μm in diameter. Norbergite was used as a standard for F, $Ba_5(PO_4)_3Cl$ for Cl, and apatite for Ca and P contents. To avoid volatile loss, F and Cl were analyzed for 10 s, whereas count times for other elements were 20 s. Fluorine and Cl were measured using the Kα line on an LDE1 and PET crystal, respectively. Analytical precision for most of the major elements was < 1%, and for F and Cl precision was ~ 5%.

Trace element contents were determined using an Agilent 7700X

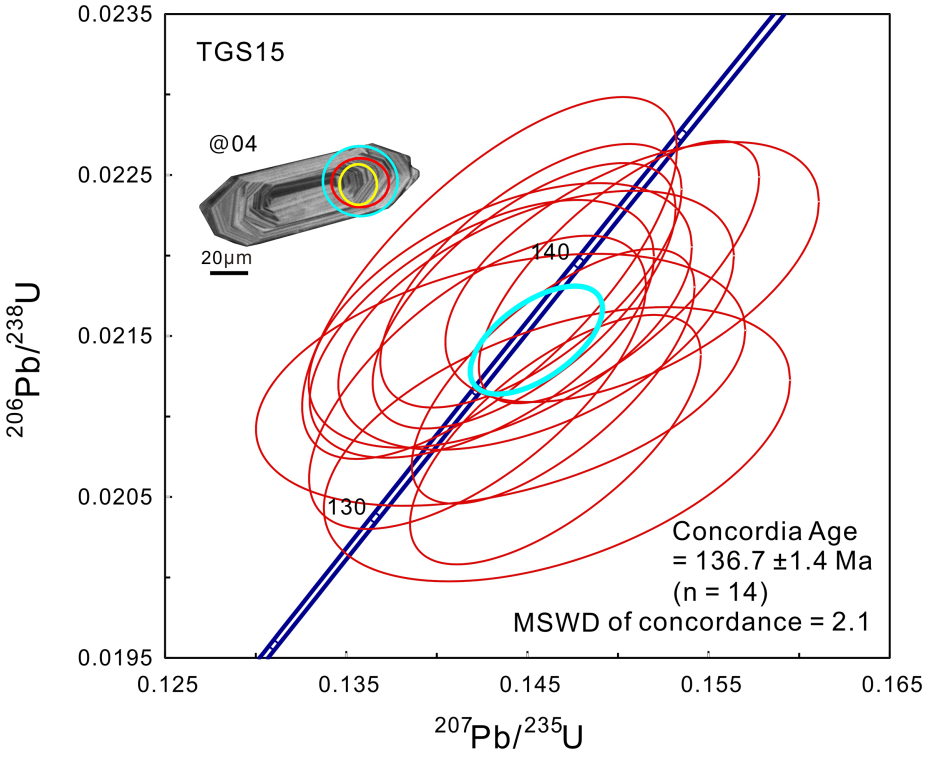

Fig. 4. SIMS zircon U–Pb Concordia diagrams for the TGS pluton. The inset shows representative zircon CL images. Circles denote the analytical spots, yellow circle represents spot of O isotope, blue circle represents spot of Hf isotope and red circle is for U–Pb dating analyses. (For interpretation of the references to color in this figure legend, the reader is referred to the web version of this article.)

ICP–MS coupled to a Resonetics 193 nm ArF excimer laser ablation system at the State Key Laboratory of Ore Deposit Geochemistry, Institute of Geochemistry, Chinese Academy of Sciences (IGCAS), Guiyang, China. In situ LA–ICP–MS analyses were performed on the positions where major element compositions were measured. Ablation used a spot diameter of 44 μm and a repetition rate of 4 Hz, and lasted for 40 s (equating to 160 pulses). Analytical procedures and instrument settings are described by Pan et al. (2016). The Ca concentration obtained by electron microprobe analysis was used as the internal standard, and the US National Institute of Standards and Technology (NIST) standard reference material (SRM) 610 was analyzed as an external standard. Analytical precision was determined by repeat analyses of NIST SRM 612 and the Madagascar and Durango apatites. Data reduction was performed using the ICPMSDataCal software (Liu et al., 2008). The precision for Mn, Sr, Nb, La, Ce, Pr, and Nd is < 10%, and for Y, Zr, Ba, Pb, Th, U, and the rest of the REEs is 10–20%.

Apatite major and trace element concentrations are shown in Supplementary material Table S5.

4. Results

4.1. Zircon U–Pb age

Zircon grains are euhedral, transparent, have prism and pyramid forms, and are 30–200 μm in length with aspect ratios of 1:1–4:1. Concentric oscillatory zoning is common in CL images (Fig. 4), and grains yield variable U (98–293 ppm) and Th (37–262 ppm) contents, with high Th/U ratios (0.32–0.99), indicating a magmatic origin. The proportion of common ^{206}Pb in the total measured ^{206}Pb (f_{206}) is 0.13%−0.50%. The U–Pb ages are all concordant within analytical error, and 14 analyses yield a concordant age of 136.7 ± 1.4 Ma (MSWD = 2.1) (Fig. 4), which represents the crystallization age of the TGS pluton.

4.2. Whole-rock geochemistry

On a QAP diagram (Fig. 5), the TGS host rocks and enclaves plot in the granodiorite and quartz monzodiorite fields. The host rocks have higher SiO_2 contents (61.2–65.3 wt%) than the enclaves (54.9–58.0 wt %). The enclaves have high MgO (4.61–6.57 wt%), $Fe_2O_3^T$ (5.65–7.26 wt%), and CaO (6.46–7.06 wt%) contents, with high Mg# (65.5–67.8), whereas, the host rocks have low MgO (1.22–1.75 wt%) (except for one sample with MgO = 0.48 wt%), $Fe_2O_3^T$ (2.82–4.75 wt %) and CaO (3.91–6.04 wt%) contents, and Mg# (41.1–52.5, apart from one sample with Mg# = 28.4). Both the host rocks and enclaves have low K_2O (1.76–1.96 wt% and 1.97–2.80 wt%, respectively) and high Na_2O (4.08–4.68 wt% and 4.63–5.11 wt%, respectively) contents. The samples plot mainly along the boundary between the high-K and medium-K calc-alkaline series on an SiO_2 versus K_2O diagram (Fig. 6a). The Na_2O, MgO, CaO and Al_2O_3 contents decrease with increasing SiO_2 contents (Fig. 6).

On a Chondrite-normalized REE diagram (Fig. 7a), the samples are enriched in light rare earth elements (LREEs) relative to heavy rare earth elements (HREEs) ($(La/Yb)_N$ = 14.5–23.0, where the subscript N denotes the Chondrite-normalized values), and exhibit no negative Eu anomaly (δEu = 0.92–1.00). The HREEs are not internally fractionated, with $(Dy/Yb)_N$ ratios of 1.42–1.57. On the primitive mantle-normalized trace-element diagram (Fig. 7b), the samples are characterized by enrichment in large ion lithophile elements (LILEs; e.g., Rb, Th and U) and depleted in heavy field strength elements (HFSEs), with pronounced negative Rb, Nb, Ta and Ti anomalies. In addition, the samples have low Y and high Sr contents, with high Sr/Y ratios (56–123). There is no obvious relationship between SiO_2 and Sr contents (Fig. 6g). The enclaves have higher Cr (148–239 ppm) and Ni (115–185 ppm) contents than the host rocks (Cr = 7.49–9.32 ppm, Ni = 4.14–11.5 ppm) (Fig. 6h).

4.3. Zircon Hf–O isotopic compositions

In situ Hf–O isotopic analyses were conducted on the same zircon grains that were U–Pb dated (see Section 4.1). Zircon from the host rock has initial $^{176}Hf/^{177}Hf$ ratios (0.282070–0.282362), corresponding to $\varepsilon_{Hf}(t)$ values of −21.9 to −11.6 (Fig. 8) and T_{DM}^C ages of 2.56–1.92 Ga. The zircon has relatively homogeneous O isotopic ratios

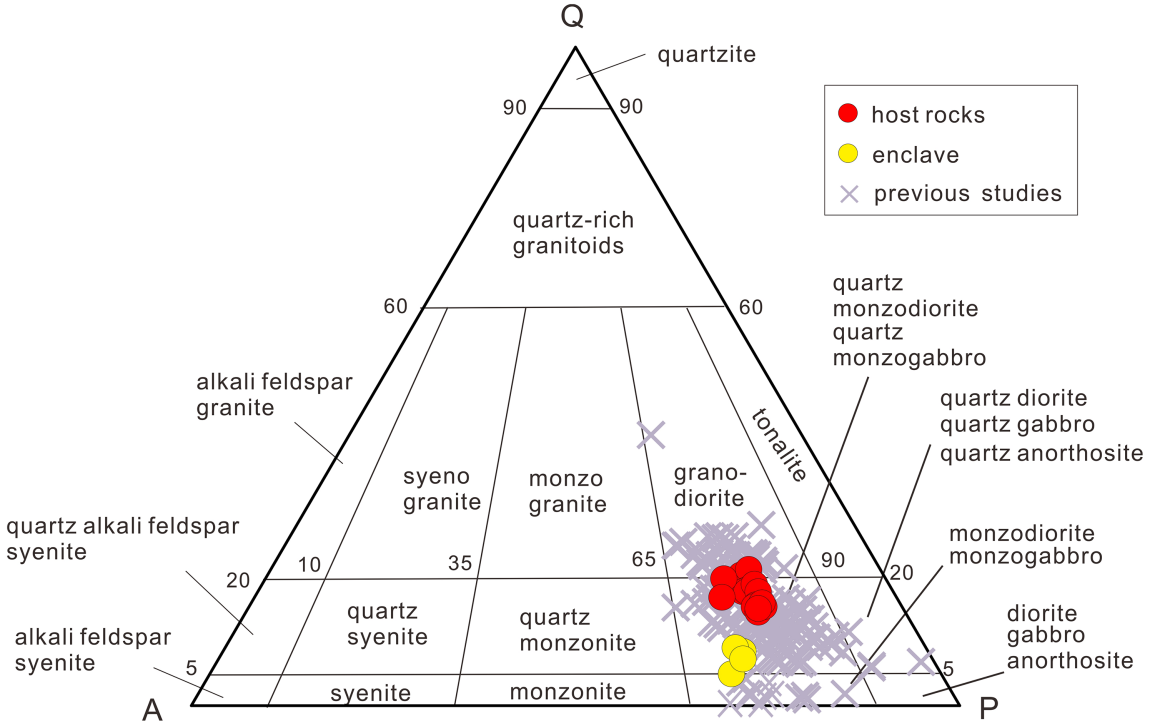

Fig. 5. QAP classification diagram for TGS granodiorite (after Le Bas and Streckeisen, 1991). The data of previous studies are in Supplementary material Table S6.

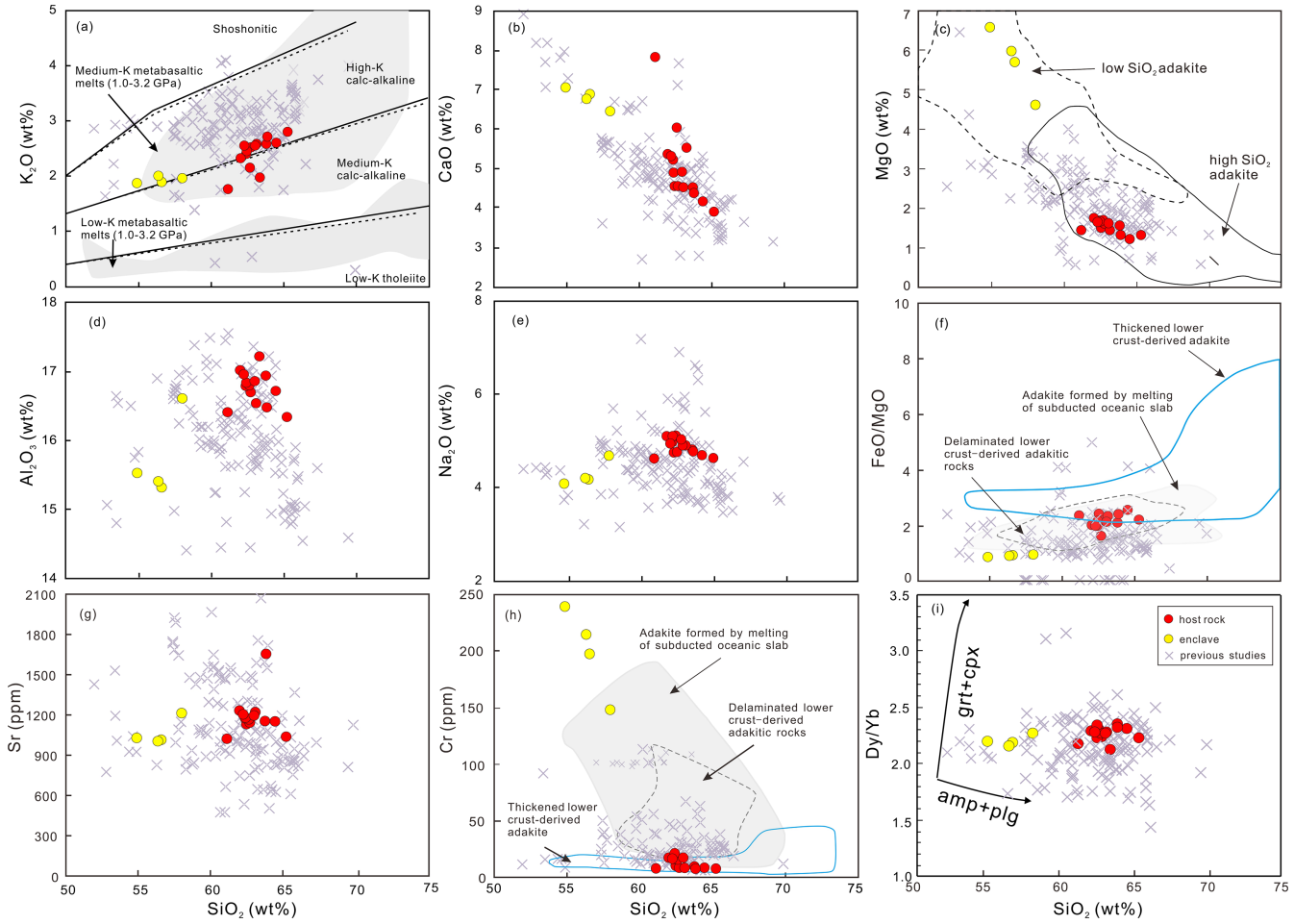

Fig. 6. SiO_2 variation diagrams of representative elements and element ratios for samples from the TGS pluton. Plot of MgO wt.% versus SiO_2 wt.% showing some of the chemical differences between low silica adakite (dotted field) and high silica adakite (solid field) varieties (modified after Castillo, 2012). Fields of adakite-formed by melting of subducted oceanic slab, delaminated lower crust-derived adakitic rocks and thickened lower crust-derived adakite are from Wang et al. (2006). The data of previous studies are in Supplementary material Table S6.

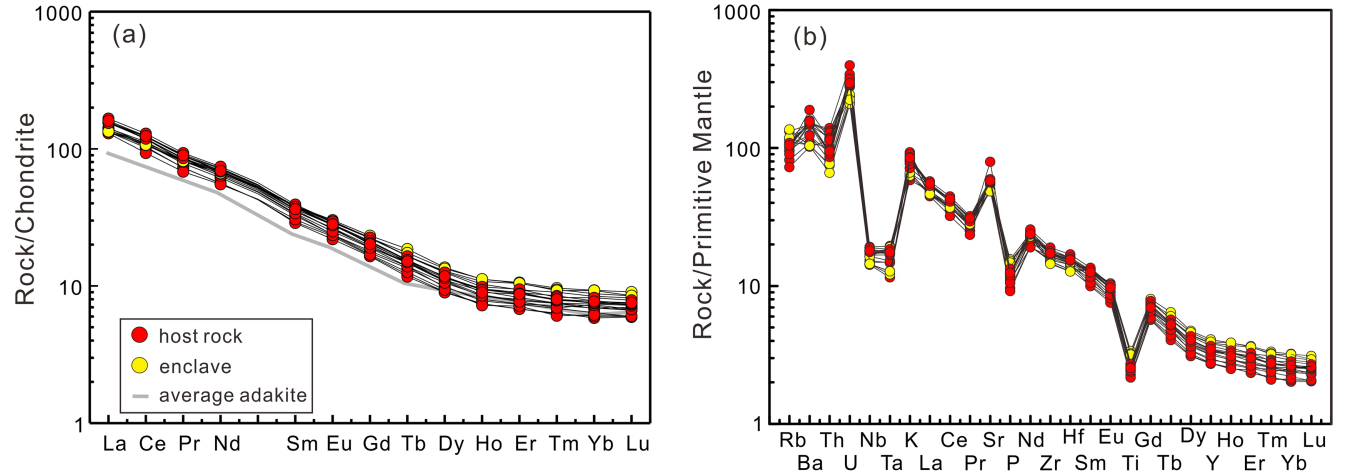

Fig. 7. Chondrite-normalized REE patterns and primitive mantle normalized incompatible element spider diagrams for the igneous rocks from the Tongguanshan. Data for normalization are from Sun and McDonough (1989). Average element concentrations of adakites in subduction zone settings are from Shimoda (2009). The literature data are summarized in Supplementary material Table S6.

($\delta^{18}O_{zircon}$ = 6.8‰–7.6‰ relative to the standard V-SMOW; Fig. 8). Zircon grains from the enclave have variable initial $^{176}Hf/^{177}Hf$ ratios (0.282022–0.282309), corresponding to $\varepsilon_{Hf}(t)$ values of −23.6 to −13.4 (Fig. 8) and T_{DM}^{C} ages of 2.57–2.06 Ga. In situ O isotopic analyses yield relatively heterogeneous O isotopic compositions ($\delta^{18}O_{zircon}$ = 6.9‰–7.3‰; Fig. 8).

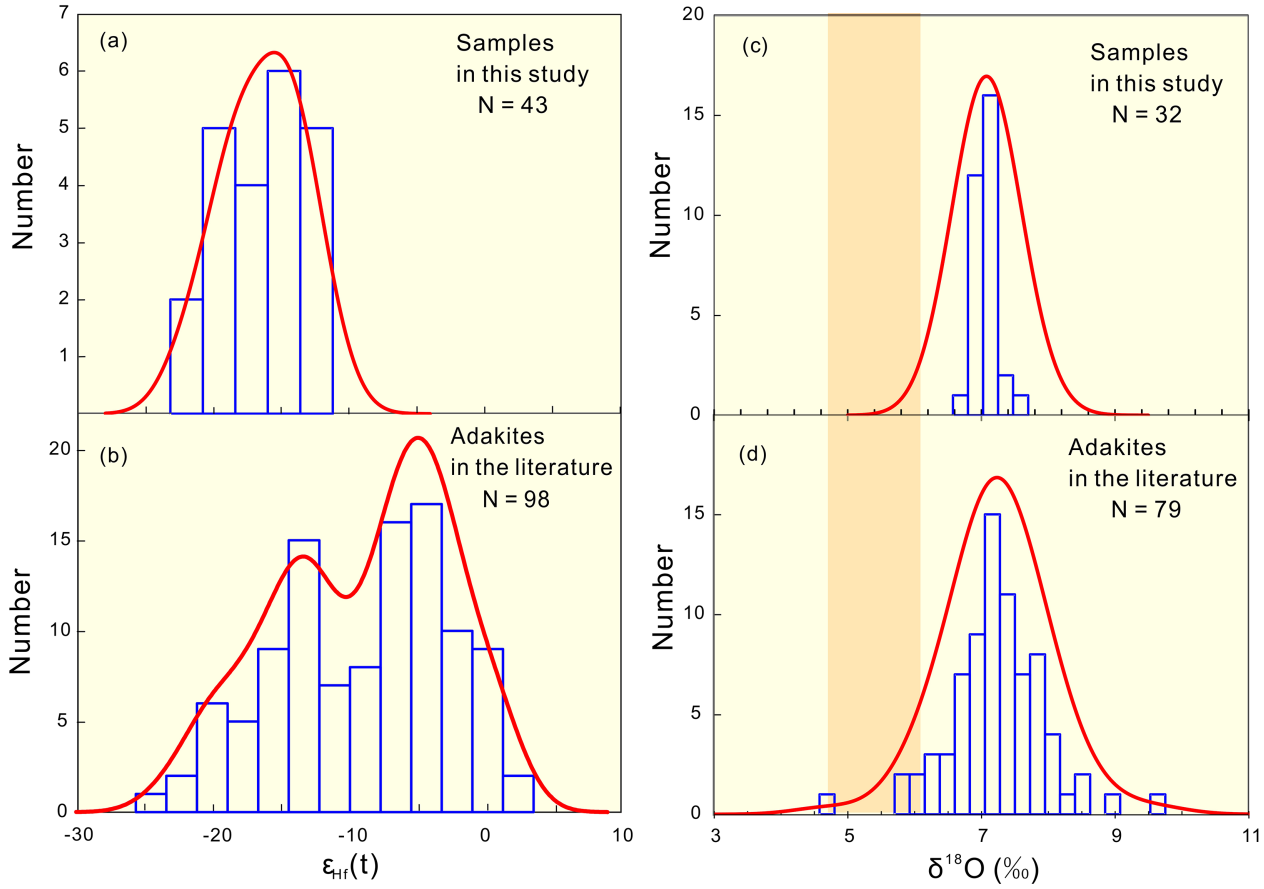

Fig. 8. In situ zircon Hf–O isotopic compositions of Mesozoic adakitic rocks in TGS. The vertical orange bars represent the normal-mantle $\delta^{18}O_{zrc}$ range. Data are reported in Supplementary material Tables S3 and S7. (For interpretation of the references to color in this figure legend, the reader is referred to the web version of this article.)

4.4. Whole-rock Sr–Nd isotopic compositions

The whole-rock Sr–Nd isotopic compositions of three representative samples were analyzed. The Sr and Nd isotopic compositions both have narrow ranges, and plot between the compositions of mid-ocean ridge basalt (MORB), marine sediments and Yangtze lower crust (Fig. 9). The host rocks have $^{87}Rb/^{86}Sr$ ratios of 0.15–0.16 and $^{87}Sr/^{86}Sr$ ratios of 0.70762–0.70763, corresponding to an initial $^{87}Sr/^{86}Sr$ ratio (I_{Sr}) = 0.7073. The $^{147}Sm/^{144}Nd$ ratios are 0.1038–0.1045 and the $^{143}Nd/^{144}Nd$ ratios are 0.51197–0.51198, corresponding to $\varepsilon_{Nd}(t)$ value of −11.4 to −11.2. The enclave sample has a $^{87}Rb/^{86}Sr$ ratio of 0.19 and a $^{87}Sr/^{86}Sr$ ratio of 0.70720, corresponding to I_{Sr} of 0.7068. The enclave also has a $^{147}Sm/^{144}Nd$ ratio of 0.1077 and a $^{143}Nd/^{144}Nd$ ratio of 0.51206, with an $\varepsilon_{Nd}(t)$ value of −9.7.

4.5. Apatite geochemistry

Most apatite grains from the TGS rocks are euhedral and are interpreted to be a magmatic origin (F > 1 wt%). Apatite grains from the host rock yield higher F (2.10–2.89 wt%) and lower Cl (0.23–0.79 wt%) contents than the those from the enclave (F = 1.10–2.79 wt%, Cl = 0.12–2.06 wt%), and there is a linear relationship between F and Cl contents (Fig. 10a). Other than the volatile elements, there are no significant compositional differences between apatites from the two samples. Chondrite-normalized apatite trace element patterns are shown in Fig. 10b. Apatite from the host rock and the enclave yield similar REE patterns enriched in LREE and depleted in HREE, with negative Eu anomalies (Fig. 10b). On an REE discrimination diagram, the apatites plot in the mantle source field (Fig. 10c). The apatite crystals have a narrow range of moderately negative Eu anomalies (δEu = 0.39–0.85; Fig. 10d). Apatite grains from the enclave have higher total REE concentrations (11,050–30,121 ppm) and lower $(La/Yb)_N$ ratios (46.3–97.0) than those from the host rock (total REE = 10325–19943 ppm, $(La/Yb)_N$ = 59.2–140). The apatite have high, variable Sr contents, and those from the host rock have lower Sr (497–665 ppm) and Y (84–259 ppm) contents than those from the enclave (Sr = 422–1805 ppm, Y = 173–397 ppm). The apatite REE contents vary by up to 100 times more than those of the bulk rock, but typically show similar patterns.

Apatite Mn contents were used to determine the redox state of granitic magmas (e.g., Chu et al., 2009; Miles et al., 2014; Sha and Chappell, 1999). A strong negative linear correlation exists between apatite Mn concentrations and oxygen fugacity (f_{O2}), represented by the equation $\log f_{O2}$ = −0.0022 (± 0.0003) Mn (ppm)–9.75 (± 0.46) (Miles et al., 2014). Apatites from the host rock have MnO contents of 0.08–0.22 wt%, which yield $\log f_{O2}$ values from −9.8 to −12.9, whereas apatites from the enclave have lower MnO contents (0.00–0.15 wt%), which yield a narrower range of $\log(f_{O2})$ values (−10.4 to −12.3).

5. Discussion

5.1. Classification of the high-silica and low-silica adakites

The host rocks and enclaves are characterized by high Sr (1040–1672 ppm), low Y (12.4–18.6 ppm) and Yb (0.99–1.58 ppm) contents, high Sr/Y (56–123) and $(La/Yb)_N$ (14.5–23) ratios (Fig. 11a and b), which are typical characteristics of adakites (Drummond and

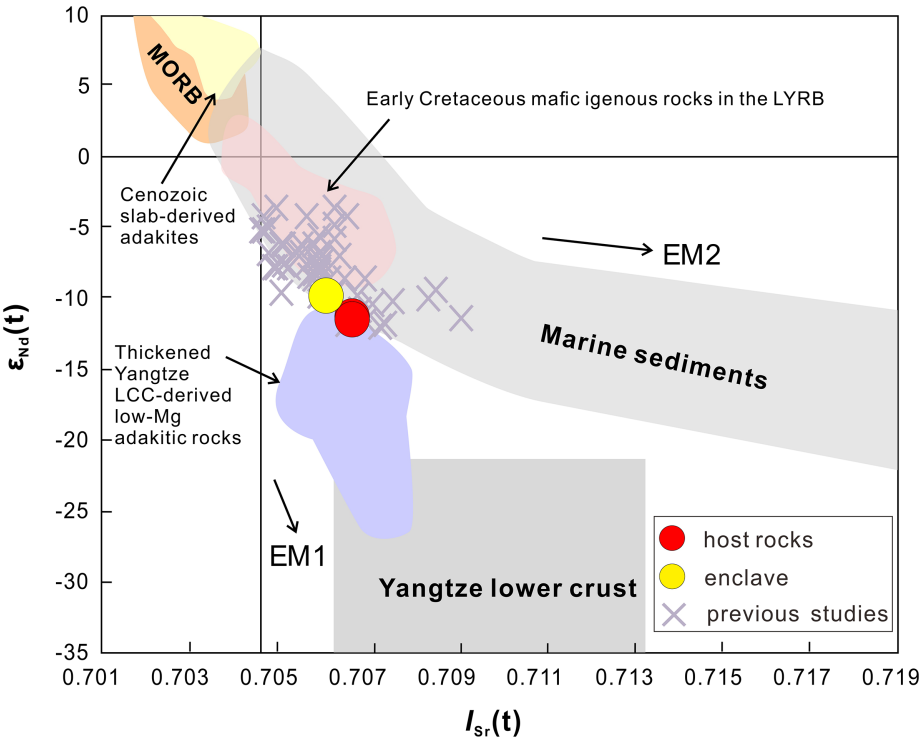

Fig. 9. Initial Sr–Nd isotopic compositions of adakites from Tongguanshan intrusions, LYRB. Data sources: Cenozoic slab-derived adakites (Defant and Kepezhinskas, 2001), thickened Yangtze lower crust-derived low-Mg adakitic rocks (Wang et al., 2004, 2007; Guo et al., 2004; He et al., 2011), early Cretaceous mafic igneous rocks in the LYRB (Yan et al., 2008), MORB and marine sediments (Hofmann, 2003), Yangtze lower crust (Jahn et al., 1999). Literature data are in Supplementary material Table S8.

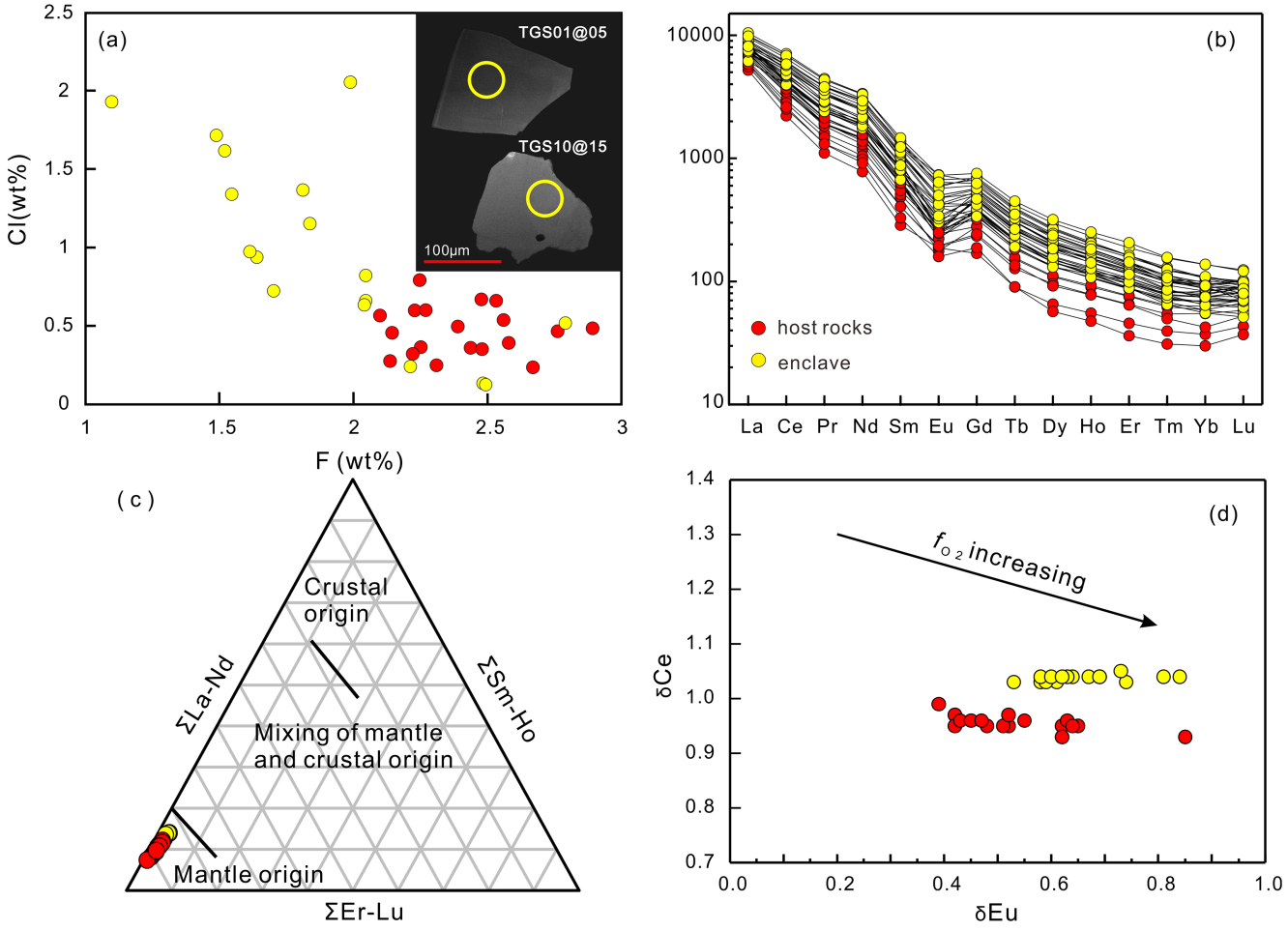

Fig. 10. Apatite (a) F versus Cl variation diagram; (b) Chondrite normalized REE diagram; (c) REE triangular diagram (Zhu et al., 2004); (d) δCe vs. δEu values variation diagram.

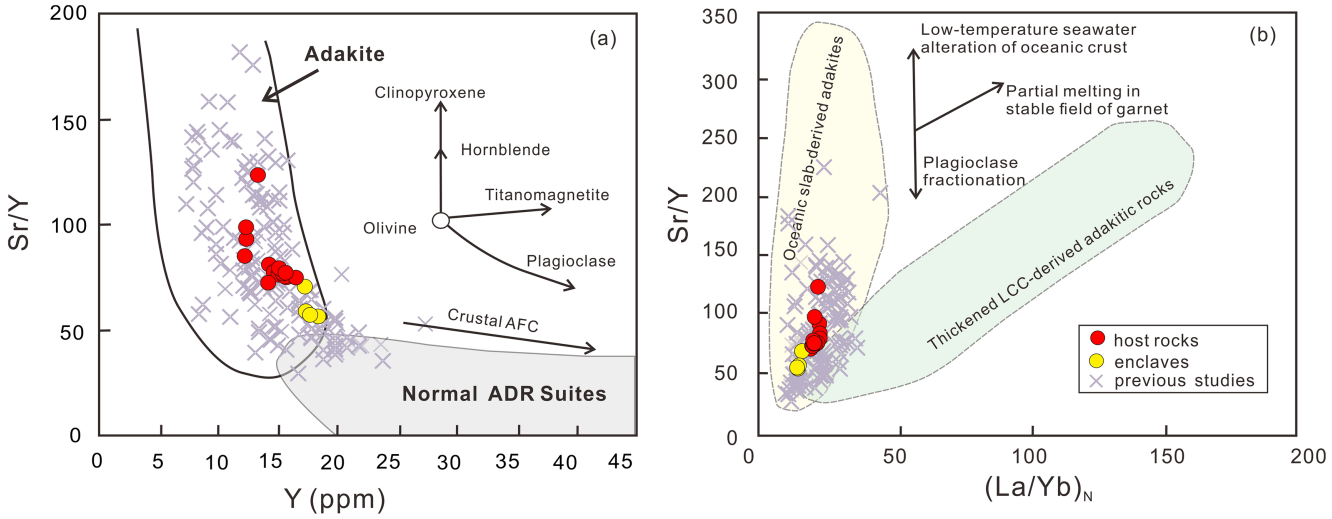

Fig. 11. (a) Sr/Y versus Y classification diagram for identifying adakitic rocks (Defant and Drummond, 1990); (b) Sr/Y versus $(La/Yb)_N$ discriminant diagram to distinguish lower crust-derived adakitic rocks from slab-derived adakites (Defant and Drummond, 1990; Liu et al., 2010). $(La/Yb)_N$ ratios are Chondrite-normalized values (Sun and McDonough, 1989). The data of previous studies are in Supplementary material Table S6.

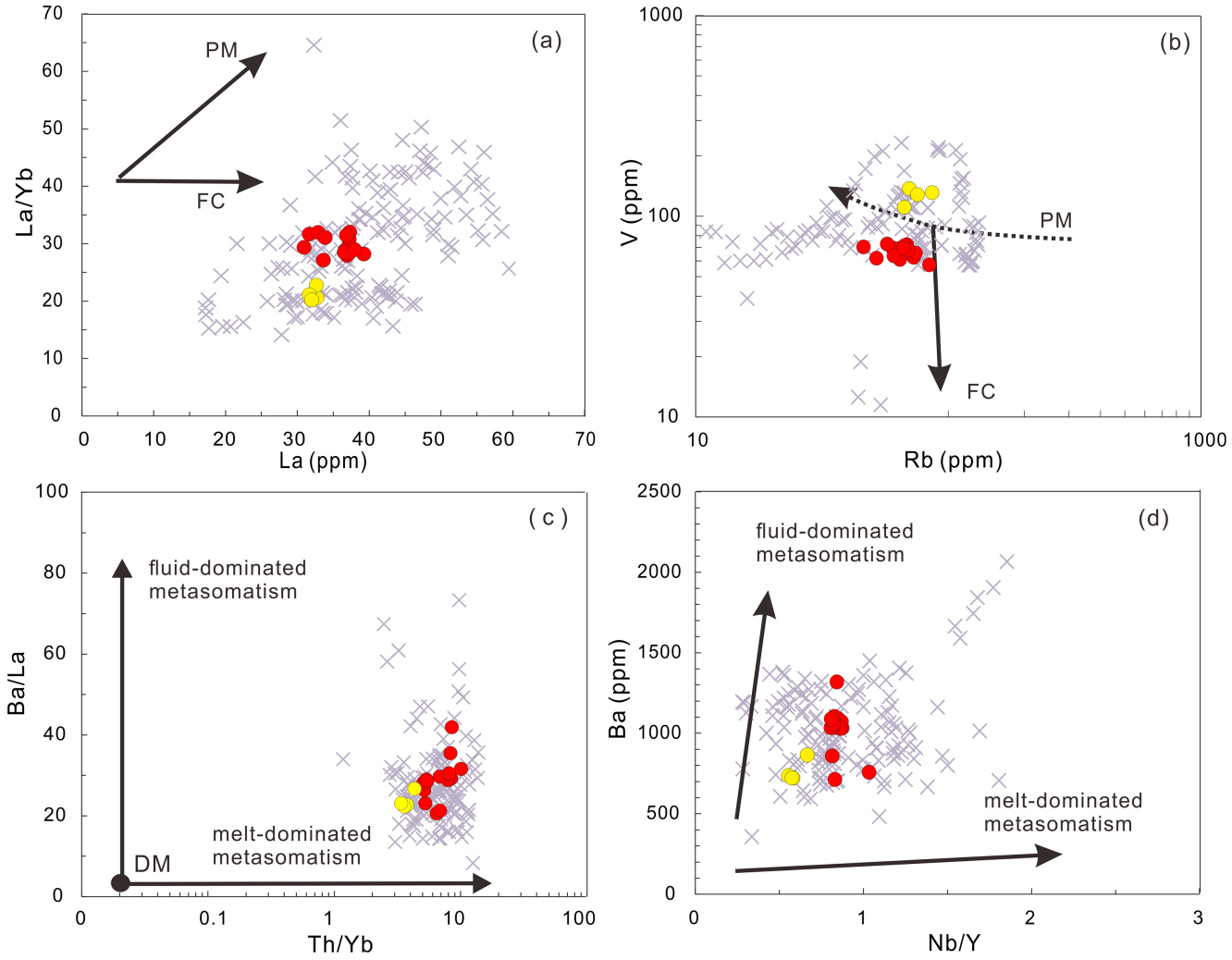

Fig. 12. Plots of (a) La versus La/Yb, (b) V versus Rb, (c) Th/Yb vs. Ba/La diagram ; (d) Ba versus Nb/Y diagram (Kepezhinskas et al. 1997). Data source: Depleted Mantle (DM) (Workman and Hart, 2005). Note: PM-partial melting, FC-fractional crystallization. Previous data in Supplementary material Table S6.

Defant, 1990). Adakites can be further classified into two groups: high-silica (HSA, SiO_2 > 60 wt%) and low-silica (LSA, SiO_2 < 60 wt%) adakites (Martin et al., 2005). HSA is thought to be the products of partial melting of a hydrous subducted slab, whereas LSA is thought to be generated by partial melting of peridotitic mantle wedge metasomatized by HSA or subduction dehydration fluids (Martin et al., 2005; Moyen and Martin, 2012; Hernández-Uribe et al., 2020). The TGS host rocks have high SiO_2 (> 62 wt%), and low MgO (< 1.75 wt%) and CaO + Na_2O (< 11 wt%) contents. In contrast, the enclaves have low SiO_2 (54.9–58.0 wt%), and high in MgO (4.61–6.57 wt%) and CaO + Na_2O (11.0–11.1 wt%) contents. The host rocks and enclaves plot in the HSA and LSA fields, respectively (Fig. 6c).

5.2. Magmatic process: Fractional crystallization, partial melting, or magma mixing?

Geochemical variations in magmatic rocks can be used to identify magmatic processes such as fractional crystallization (FC), partial melting (PM), and magma mixing. If the host rocks are formed through the FC of the magma found in the enclaves, then there should be a continuous compositional trend from the enclaves to host rocks. However, the major and trace element compositions of the enclaves and host rocks cannot be explained by this process (Figs. 6, 7 and 11). The field, petrological, and chemical data favor magma mixing in TGS adakites. The distribution, shape, and color of the microgranular enclaves and their contacts with the host rocks (back veins and no chilled margins) indicate that the two magmas coexist (Xu et al., 2004; Chen et al., 2016; Du et al., 2018). Abundant disequilibrium textures, such as embedded crystal structure of plagioclases and hornblendes, and acicular apatites, as well as plagioclase and hornblende compositions, suggest at least one episode of magma mixing (Zhao et al., 2012; Chen et al., 2016). The presence of abundant microgranular mafic enclaves and amphibole megacrysts in the host rocks indicate that magma mixing may have taken place in the shallow chamber (Wu et al., 2000; Qin et al., 2003; Chen et al., 2016). In addition, previous studies found inherited late Archean zircons in TGS adakites, indicating the assimilation of ancient crustal materials (Xie et al., 2018), possibly from the basement rocks of the Archaean Kongling group (Zhang et al., 2006; Guo et al., 2014) and the Douling complex (Hu et al., 2013).

Correlation diagrams between compatible, moderately incompatible, and highly incompatible trace elements are effective in distinguishing FC from PM in the evolution of magmatic system. The correlations between La contents and La/Yb ratios and between Rb and V contents (Fig. 12a and b) suggest that the compositions of both the host rocks and enclaves are controlled more by the degree of PM rather than FC. Yttrium is moderately incompatible to slightly compatible in amphibole in a basaltic system, and moderately incompatible in the other major minerals such as olivine, pyroxene, biotite, and plagioclase in basaltic to dacitic systems, but becomes highly compatible in amphibole in melts with high silica contents (Ewart and Griffin, 1994; Sisson, 1994; Prowatke and Klemme, 2005; Richards and Kerrich, 2007). The trend in the Y vs Sr/Y diagram (Fig. 11a) also suggests that FC was not the dominant process causing the chemical variation in the host rocks and the enclaves.

5.3. Petrogenesis of the host rocks and enclaves in TGS

5.3.1. Petrogenesis of the host rock: Partial melting of subducted oceanic crust

Adakites with different origins show different geochemical characteristics, such as MgO contents, and K_2O/Na_2O, Sr/Y, and $(La/Yb)_N$ ratios. Adakites derived from partial melting of the subducted oceanic crust are usually characterized by high Na_2O and low K_2O contents (Defant and Drummond, 1990; Moyen, 2009), similar to our samples (Na_2O > 4 wt%, K_2O < 2.8 wt%, K_2O/Na_2O = 0.38–0.57). However, adakites derived from partial melting of thickened lower continental crust can also have Na_2O-rich compositions (Petford and Atherton, 1996; Xiong et al., 2011). Other geochemical tests are needed to distinguish between adakites produced by partial melting of oceanic and continental crust (Liu et al., 2010; Ling et al., 2011; Sun et al., 2012; Deng et al., 2016, 2019).

A positive correlation between $(La/Yb)_N$ and Sr/Y ratios can be observed in the adakites produced by different degrees of partial melting of thickened or delaminated LCC with a garnet amphibolite or eclogite residue (Fig. 11b), as observed in adakites from the Dabie Mountain and areas adjacent to the South Tan–Lu fault, eastern China (Liu et al., 2010; Ling et al., 2011; Sun et al., 2012; Luo et al., 2018). However, in modern subduction zones, adakites originating from the melting of oceanic crust have high and variable Sr/Y ratios but considerably lower $(La/Yb)_N$ ratios than those of the LCC (Sun et al., 2008, 2012; Liu et al., 2010; Rudnick and Gao, 2014). The adakites in TGS are characterized by low $(La/Yb)_N$, and high and variable Sr/Y ratios, and overlapped with the compositions of Circum-Pacific adakites, which formed via the melting of subducted oceanic crust (Fig. 11). The most recent study by Hernández-Uribe et al. (2020) also proposed that partial melting of the subducted hydrothermally altered basalt can produce magma with geochemical signatures of HSA. Besides, the TGS adakites show isotopic compositions strikingly different from those of the LCC basement rocks of the Yangtze Craton, as represented by the Archean Kongling Group ($\varepsilon_{Nd}(t) < -25$, $\varepsilon_{Hf}(t) < -60$; t = 140 Ma; Guo et al., 2014). Thus, the derivation from the continental crust model is excluded.

Adakite REE patterns and trace element ratios reflect the mineral assemblage in their source areas (Goss and Kay, 2009; König and Schuth, 2011; Ma et al., 2015). Previous experimental studies suggest that differentiated and HREE-depleted REE patterns are products of either low-degree (< 10%) partial melting of amphibolite, garnet-amphibolite, eclogite in which hornblende or garnet are essential residual phases, or hornblende-controlled fractionation of hydrous basaltic magma (Rapp et al., 1991; Rapp and Watson, 1995). The TGS adakites have REE patterns that are transitional between garnet-dominant and hornblende-dominant patterns (Fig. 7), which suggest that both garnet and hornblende are in the residual phases, consistent with the partial melting of garnet amphibolite or amphibole eclogite (Deng et al., 2019).

The enrichment in Sr and absence of negative Eu anomalies, together with the depletion in Y and HREE (Fig. 7) and highly variable $(La/Yb)_N$ ratios (Fig. 11), indicate the existence of residual garnet rather than residual plagioclase (Defant and Kepezhinskas, 2001). Garnet preferentially incorporates HREE, whereas amphibole preferentially incorporates middle rare earth element (MREE) over HREE. Therefore, melts with residual garnet have higher Dy/Yb ratios than melts with residual amphibole. The relatively constant Dy/Yb ratios with increasing SiO_2 contents (Fig. 6i) indicate that both amphibole and garnet are residual phases. If the residual material is dominated by amphibole, the melt would have a flat HREE pattern (Y/Yb ≈ 10 and $(Ho/Yb)_N \approx 1$). Otherwise, the depletion in HREE (Y/Yb > 10 and $(Ho/Yb)_N > 1.2$) would indicate garnet is the major residual phase (Hu et al., 2017). The Y/Yb (11.3–12.6) and $(Ho/Yb)_N$ (1.16–1.27) ratios of the TGS adakites suggest that garnet is the dominant residual phase.

Niobium and Ti are hosted in rutile under hydrous mantle conditions (Tatsumi, 1986). Both of these elements are strongly depleted in the TGS adakites (Fig. 7), which suggests the presence of residual rutile in the source area (Xiong et al., 2006). The high Nb/Ta (17–22, except for one sample with Nb/Ta = 14) ratios of the adakites, suggest they originated from rutile-bearing eclogite, as rutile has low $D_{Nb/Ta}$ values (~0.75; Xiong et al., 2005) that lead to high Nb/Ta ratios (> 17.6) in coexisting melts. Fe–Ti oxides such as ilmenite or Ti-magnetite have limited effects on Nb–Ta fractionation, as D_{Nb} and D_{Ta} in these minerals are similar (Green and Pearson, 1987). Besides, the Zr/Sm ratios of TGS adakites (average 36.4) are similar to other adakites (average Zr/Sm = 36.0; Shimoda, 2009) supporting the amphibole-melting model

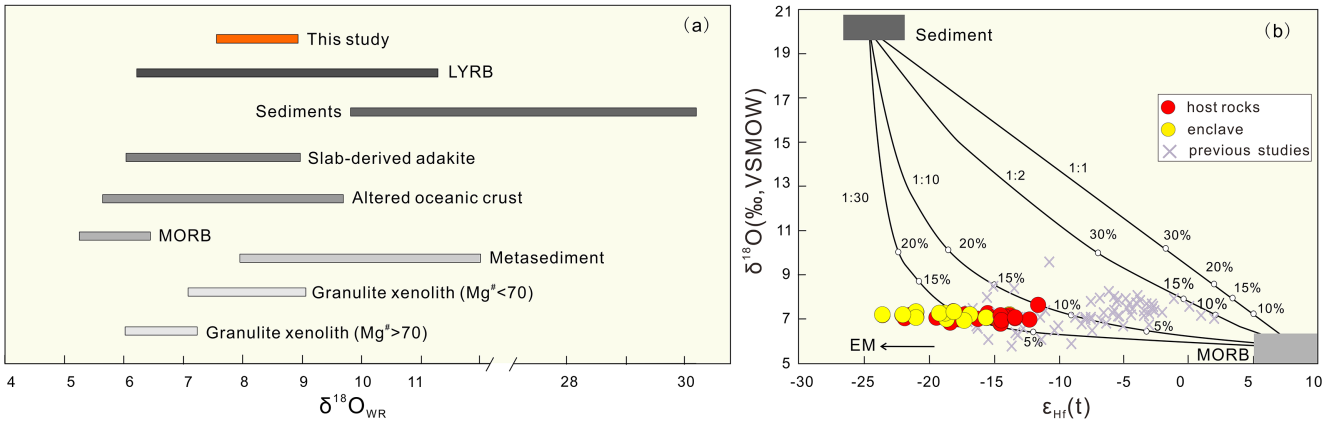

Fig. 13. (a) Integrated oxygen isotopes reservoir of the Earth. Whole-rock oxygen isotope from Tongguanshan and LYRB are calculated from $\delta^{18}O_{zrc\text{-}WR} = \delta^{18}O_{zrc} - \delta^{18}O_{WR} \approx -0.0612$ (wt% SiO_2) + 2.5 (Valley et al., 2005). Oxygen isotopes of lower continental granulite xenoliths are from Kempton and Harmon (1992), MORB is from Chauvel et al. (2008), altered oceanic crust are from Muehlenbachs (1998), slab derived adakite are from Bindeman et al. (2005) and sediments are from Hoefs (2009). (b) $\delta^{18}O$ versus $\varepsilon_{Hf}(t)$ isotopes plot of the Tongguanshan adakitic rocks (modified after Wang et al., 2013a). The data sources are Chauvel et al. (2008) and Hoefs (2009) for MORB and sediments. The endmembers are: (1) MORB: $^{176}Hf/^{177}Hf = 0.283141$, $\delta^{18}O = 5.8‰$; (2) marine sediments: $^{176}Hf/^{177}Hf = 0.282$, $\delta^{18}O = 20‰$. The mixing curves were constructed using different Hf element ratios from MORB/Sediments = 1:30 to 1:1. Previous data sources in Supplementary material Table S7.

(Foley et al., 2002). Therefore, garnet, amphibole, and rutile or Fe-Ti oxides may all exist in the source area. The source is most probably hydrous amphibole eclogite (Mahoney et al., 1998; Hou et al., 2004; Deng et al., 2019).

Incompatible trace element data for the TGS adakites indicate the involvement of an enriched components in their source melt. They show enrichment in Ba and LREE, high Zr and Hf contents relative to Sm and Y contents (Fig. 7). Contributions of terrigenous sediments could lead to more crust-like elements and radiogenic isotope ratios (e.g., Shimoda and Tatsumi, 1999; Shimoda et al., 1998, 2003). In situ zircon Hf and O isotope data provide strong evidence for the involvement of enriched material in the formation of the adakites (Figs. 8 and 13), which are consistent with the involvement of subducted sediments in the source and/or the incorporation of lower crustal material (e.g., Archean basement rocks). The $\delta^{18}O$ values of zircon from the TGS adakites overlap those of slab-derived adakites, altered oceanic crust, and metasediments, but are higher than those of the mantle (Fig. 13a). Thus, the relatively high oxygen isotopic compositions may be related to mixing between an igneous member with mantle-like $\delta^{18}O$ values and sediments characterized by heavy $\delta^{18}O$ values (Fig. 13b; Hoefs, 2009). Moreover, it has been proposed that the partial melts of sediments during subduction could mixed with partial melts of basaltic oceanic crust to generate hydrous adakitic magmas (e.g., Borisova et al., 2006).

Adakites derived from oceanic crust usually have depleted Sr isotopic compositions ($^{87}Sr/^{86}Sr < 0.7040$; Defant and Drummond, 1990). The slightly enriched Sr isotope compositions of the TGS adakites could be attributed to the involvement of ancient crustal material or sediments in their generation, as the subducted marine sediments usually have high Sr and Nd contents and highly enriched radiogenic isotopic compositions which are similar to those of the continental crust (Deng et al., 2016; Elliott et al., 1997; Plank and Langmuir, 1998; Wang et al., 2013a, 2013b). On a Sr–Nd diagram (Fig. 9), the TGS adakites and enclaves plot between MORB, marine sediment, and Yangtze lower crust compositions. Different I_{Sr} ratios of the cores and rims of plagioclase in TGS adakites have also been reported (Chen et al., 2016). Therefore, the Sr–Nd isotopic compositions also suggest mixing between more than two endmembers: slab-derived (adakitic) magmas, with contributions from both pelagic and terrigenous subducted sediments and ancient continental crust (Fig. 9). In addition, previous studies found inherited late Archean zircons in TGS adakites, indicating the assimilation of ancient crustal materials (Xie et al., 2018), possibly from the basement rocks of the Archaean Kongling group (Zhang et al., 2006; Guo et al., 2014) and the Douling complex (Hu et al., 2013). This shows that magma mixing and crustal contamination play major roles in producing the chemical variation in the TGS adakites.

Above all, the trace element and isotopic characteristics of the adakites can be explained by melting of amphibole eclogite in the oceanic crust source. Therefore, we suggest that the host rocks of TGS were primarily derived mainly from partial melting of subducted oceanic crust mixing with marine sediments, followed by interaction with enriched mantle during ascent, and the assimilation of ancient crustal material during emplacement.

5.3.2. Petrogenesis of the enclaves: Partial melting of mantle peridotite metasomatized by slab-derived melts

The enclaves in TGS pluton are basaltic-andesitic in composition and enriched in Cr and Ni concentrations, and the low Cr/Ni ratios (1.3–1.4) are close to the value of mantle peridotites (~1.5; Taylor and McLennan, 1995), indicating mantle melting genesis. They are highly enriched in LILEs such as Sr and Rb, and depleted in HFSEs such as Nb and Ti (Fig. 7b), which are the results of basaltic magmas derived from a lithospheric mantle metasomatized by fuilds/melts issuing from a subducted slab. The presence of euhedral hornblende crystals in the enclaves also suggest the parental magma was hydrous. Considering the apatite and magnetite and pyroxene compositions reported by previous study (Chen et al., 2016), both of the petrological and geochemical data support the enriched lithospheric mantle source metasomatized by slab-released fluid/melt for the mafic magma.

Ratios of highly incompatible trace element ratios often reflect source compositions because they do not change significantly during melting (McCulloch and Gamble, 1991; Hofmann, 2003; Kelley et al., 2005; Sun et al., 2008; Shellnutt and Dostal, 2019). Ta/U and Nb/U ratios are sensitive to crustal contamination and can be used to discriminate between metasomatism by slab derived-fluid and melt (Hofmann et al., 1986). The enclaves have Ta/U ratios of 0.1–0.2 and Nb/U ratios of 1.7–2.3 (crust = 1.1 and 12.1, respectively; Taylor and McLennan, 1995), which imply that the source area was metasomatized by subducted slab derived fluids or melts enriched in water-soluble elements, such as U (Kelley et al., 2005; Sun et al., 2008), rather than by continental crust melts. If the main metasomatic agent was fluid derived from slab dehydration, the resulting magma have low Nb/U ratios (~0.22), be enriched in LILE and depleted in Nb and Ta, and have high HREE contents (Martin et al., 2005), as the fluids would transfer more

LILE than HFSE (Ayers, 1998). However, this is not consistent with the geochemical features of the enclaves. Moreover, the correlation between Ba/La and Th/Yb ratios, between Ba and Nb/Y suggest modification of the source by slab-derived melts (Fig. 12c and d; Yan et al., 2020). Therefore, the enclaves are probably originated from a mantle peridotite source metasomatized mainly by slab-derived melt (Martin et al., 2005; Moyen, 2009), which can also reasonably explain the isotopic characteristics.

5.4. Implications for Cu mineralization: High oxygen fugacity and fluid compositions

Knowing the precise age of the adakites is key to understanding their relationship with the related metallogenic events. Our SIMS zircon U–Pb age of the granodiorite is 136.7 ± 1.4 Ma (Fig. 4), which represents the crystallization age of the TGS adakites. Previous studies have presented several LA–ICP–MS zircon U–Pb ages in the range of 134–143 Ma (Xu et al., 2004; Chen et al., 2016; Xie et al., 2017), overlaps to the molybdenite Re-Os mineralization ages (137–143 Ma) obtained in the Tongling region (Sun et al., 2003; Mao et al., 2006; Li et al., 2014), implying a genetic relationship between the Early Cretaceous adakites and the large-scale Cu–Au mineralization (Xu et al., 2004; Xie et al., 2009, 2017; Yang et al., 2011). Therefore, the TGS adakites can provide important information about the Cu–Au mineralization process, and aid magmatic–hydrothermal ore exploration in the Tongling region.

The magma mineralization process is influenced by the enrichment of ore-forming elements in the magma source, magma migration, magma differentiation and hydrothermal process (Zhang et al., 2018, 2019a, 2019b). Previous studies proved that the enrichment of Cu in ore deposit is mainly controlled by the copper content, oxygen fugacity and halogen content in the magma source (Nadeau et al., 2010; Sun et al., 2015; Zhang et al., 2017). Given the high Cu contents of oceanic crust melt (> 100 ppm) which is three times higher than those of the primitive mantle or the continental crust (McDonough and Sun, 1995; Rudnick and Gao, 2003; Sun et al., 2003), slab melts produced by subducted oceanic crust melting under high oxygen fugacity (> ΔFMQ + 1.5) are usually with high initial Cu contents (> 500 ppm) (Sun et al., 2013, 2016, 2017; Zhang et al., 2017). Therefore, adakites produced by partial melting of subducted oceanic crust are especially favorable for Cu mineralization.

5.4.1. High oxygen fugacity of the magma

Copper is a highly chalcophile element, and is highly compatible in sulfides. In a high oxygen fugacity environment, Cu can be liberated when sulfur is extracted as sulphate during partial melting, and then enriched in the melt during differentiation before partitioning into an exsolved fluids phase (Sun et al., 2003, 2015, 2017; Nadeau et al., 2010). Magma oxygen fugacity controls on the abundance and oxidation state of sulfur in magmas, which directly controls the partitioning and transport of Cu in magmas before mineralization (Ballard et al., 2002; Sun et al., 2003; Zhang et al., 2017). This is supported by the empirical association between Cu–Au deposits and adakitic intrusions in subduction zones around the world (e.g., Thiéblemont et al., 1997; Oyarzún et al., 2001).

The enrichment in LREE relative to HREE and negative Eu anomalies (Fig. 10b) of the apatite may be the result of either Eu depletion in the host melt or an oxidized magma (Pan et al., 2016). The adakitic affinity of the melt precludes the inheritance of the negative Eu anomalies from the host melts, suggesting that the negative Eu anomalies are related to the oxidation state of the magma. The weakly negative correlation between δEu and δCe in the apatite samples indicates the TGS Cu–Au polymetallic-bearing magmas were originated in a high oxygen fugacity environment (Fig. 10d; Chu et al., 2009; Ding et al., 2015; Xie et al., 2018; Qian et al., 2019), also by the logf_{O2} values estimated from apatite compositions (granodiorite = −9.8 to −12.9, enclave = −10.4 to −12.3) obtained using the equation from Miles (2014). Previously reported high Ce^{4+}/Ce^{3+} and high Eu/Eu* ratios of zircon from the adakites also suggest a high f_{O2} (Wang et al., 2013a, 2013b; Hu et al., 2017; Xie et al., 2017). The subducted altered oceanic crust may be hydrous and oxidized (Liu et al., 2010), which potentially favor Cu–Au mineralization.

5.4.2. Halogen compositions of the metasomatic fluid

Fluorine and Cl play an important role during magmatic evolution by depolymerizing the melt structure and enabling hydrothermal metal transport and ore deposition during degassing and fluid exsolution (Dingwell et al., 1998; Filiberto and Treiman, 2009; Harlov, 2015). Apatite is the main buffer of F and Cl contents in the melt. The partitioning of F and Cl in igneous apatite depends mostly on the initial melt composition, and is not strongly influenced by fractional crystallization or susceptible to subsolidus halogen exchange (Sha and Chappell, 1999; Mathez and Webster, 2005). Therefore, F and Cl contents and ratios of apatite reflect the halogens in the system from which it crystallized (Jiang et al., 2018a).

The mantle usually has low Cl contents (< 0.1 wt%), and is not significantly influenced by Cl recycling (Lassiter et al., 2002). Apatite that crystallized from supracrustal material would also have low Cl contents because sediment lose more Cl than F during weathering (Blevin and Chappell, 1992). The apatite from the host rocks has higher F (2.10–2.89 wt%) and lower Cl (0.23–0.79 wt%) than that of the enclaves (F = 1.10–2.79 wt%, Cl = 0.12–2.06 wt%; Fig. 10a). The apatite from the enclaves generally has higher Cl/F ratios (0.05–1.76, with most > 0.30) than that of the host rocks (0.09–0.35, with only one > 0.30). However, apatite from both of them have higher Cl/F ratios than those in magmas derived from anatexis of continental crust which have extremely low Cl/F ratio (Qian et al., 2019). This suggests that the relatively high apatite Cl contents are neither the result of the addition of mantle-derived materials, nor the product of partial melting of supracrustal material. During slab dehydration, Cl is highly incompatible and preferentially enters the liquid phase (Stroncik and Haase, 2004). Fluids or melts derived from a subducted slab are probably the source of Cl (Kendrick et al., 2011; Kawamotoa et al., 2013; Reynard, 2013; Jiang et al., 2018a) in the TGS adakites, which is consistent with the other geochemical characteristics. Combining our results with those of recent studies on apatite from ore-bearing intrusive rocks (Qian et al., 2019), we suggest that slab-derived fluids or melts, which have high Cl/F ratios, are involved in the generation of the parental magmas of the TGS pluton.

Copper is more sensitive to Cl than to F, and is thought to partition into Cl-rich oxidized aqueous fluids in the form of chloride complexes or as HS-bearing ligands in moderate salinity fluids (Candela and Holland, 1986; Gammons and Williams-Jones, 1997; Gibert et al., 1998; Hedenquist and Lowenstern, 1994; Noll et al., 1996; Sun et al., 2004). The increase in the Cl content will markedly increase their solubility (Bai and Koster Van Groos, 1999; Hezarkhani et al., 1999; Archibald et al., 2001). Therefore, Cl-rich fluids are critical for the transportation of these metals (Bai and Koster Van Groos, 1999) and necessary for the formation of Cu–Au deposits. Furthermore, high f_{O2} fluids and melts enriched in volatile elements (e.g., S) and ore-forming elements (Cu and Au) might be released during the partial melting of the subducted slab (Mungall, 2002).

The slab-derived fluids or melts metasomatized oceanic crust and mantle peridotite, and underwent the addition of marine sediments, magma mixing and crustal contamination, generating high f_{O2} and Cl-rich adakitic magmas in TGS. This magma enhanced the extraction and transportation of the Cu and Au that ultimately formed the Cu–Au polymetallic deposits in TGS. The integration of our data with geochemical data from previous studies suggest that other large-scale Cu–Au polymetallic mineralization in the LYRB might also be produced by the same mechanism as the TGS deposit.

6. Conclusions

Based on zircon U–Pb geochronology, and the whole-rock major and trace element and Hf–O–Sr–Nd isotopic compositions of the intrusive rocks of the Tongguanshan Cu–Au deposit in the Tongling region, along with data from the other Early Cretaceous adakites in the Lower Yangtze River Belt, we draw the following conclusions:

(1) The Tongguanshan host rocks and enclaves are granodiorite and quartz monzodiorite. Their compositions show adakitic affinities, with high Sr and low Y and Yb contents, and high Sr/Y and $(La/Yb)_N$ ratios. The host rocks and enclaves can be further classified as high-silica (SiO_2 = 61.2–65.3 wt%) and low-silica (SiO_2 = 54.9–58.0 wt%) adakites, respectively.
(2) High precision zircon U–Pb age suggests that the host rock crystallized at 136.7 ± 1.4 Ma, coeval with the enclave, and the mineralization in the Tongling region. This implies a close temporal and genetic relationship between the intrusive rocks and the regional Cu–Au mineralization.
(3) Field observations, and isotopic and mineral compositions suggest the magma mixing and crustal assimilation. Integrating our data with other geochemical data, we propose that the adakites are formed by the partial melting of a subducted oceanic slab mixed with marine sediments, followed by the assimilation of lower crustal material during magma ascent. The enclaves are the products of partial melting of mantle peridotite metasomatized by slab-derived materials, also influenced by crustal assimilation.
(4) The high f_{O2}, systematically varying high Cl contents, and high Cl/F ratios of the apatite in the TGS adakites indicate an oxidized and slab-derived volatile enriched environment, which are conductive to large-scale Cu–Au mineralization.

Declaration of Competing Interest

The authors declare that they have no known competing financial interests or personal relationships that could have appeared to influence the work reported in this paper.

Acknowledgements

This contribution was financially supported by the National Key R&D Program of China (2016YFC0600408), National Natural Science Foundation of China (41703010), the CAS 'Light of West China' Program, the Taishan Scholar Program of Shandong (ts201712075), and AoShan Talents Cultivation Program(2017ASTCP-OS07). We are appreciative of the efforts made by Chief Editor Franco Pirajno, Hélène Legros and two anonymous reviewers to help us improve this manuscript. Saijun Sun and Zhekun Zhang are acknowledged for logistical support during the fieldwork. We also thank Boqin Xiong, Qin Yang, Wanfeng Zhang, Yanqiang Zhang, Le Zhang and Peijun Lin for technical assistance with SIMS, MC-LA-ICPMS and EMPA.

Appendix A. Supplementary data

Supplementary data to this article can be found online at https://doi.org/10.1016/j.oregeorev.2020.103717.

References

Archibald, S.M., Migdisov, A.A., Williams-Jones, A.E., 2001. The stability of Au-chloride complexes in water vapor at elevated temperatures and pressures. Geochim. Cosmochim. Acta 65, 4413–4423.
Ayers, J., 1998. Trace element modeling of aqueous fluid – Peridotite interaction in the mantle wedge of subduction zones. Contrib. Miner. Petrol. 132, 390–404.
Bai, T.B., Koster Van Groos, A.F., 1999. The distribution of Na, K, Rb, Sr, Al, Ge, Cu, W, Mo, La, and Ce between granitic melts and coexisting aqueous fluids. Geochim. Cosmochim. Acta 63, 1117–1131.
Ballard, J.R., Palin, M.J., Campbell, I.H., 2002. Relative oxidation states of magmas inferred from Ce(IV)/Ce(III) in zircon: Application to porphyry copper deposits of northern Chile. Contrib. Miner. Petrol. 144, 347–364.
Bao, Z.A., Chen, L., Zong, C.L., Yuan, H.L., Chen, K.Y., Dai, M.N., 2017. Development of pressed sulfide powder tablets for in situ sulfur and lead isotope measurement using LA-MC-ICP-MS. Int. J. Mass Spectrometry.
Barth, A.B., Walshe, J.L., Cloutier, J., Verrall, M., Cleverley, J.S., Pownceby, M.I., Macrae, C.M., Wilson, N.C., Tunjic, J., Nortje, G.S., Robinson, P., 2013. Biotite and apatite as tools for tracking pathways of oxidized fluids in the Archean East Repulse Gold Deposit. Australia. Econ. Geol. 108, 667–690.
Bindeman, I.N., Eiler, J.M., Yogodzinski, G.M., Tatsumi, Y., Stern, C.R., Grove, T.L., Portnyagin, M., Hoernle, K., Danyushevsky, L.V., 2005. Oxygen isotope evidence for slab melting in modern and ancient subduction zones. Earth Planet. Sci. Lett. 235, 480–496.
Blevin, P.L., Chappell, B.W., 1992. The role of magma sources, oxidation states and fractionation in determining the granite metallogeny of eastern Australia. Earth Environ. Sci. Trans. Royal Soc. Edinburgh 83 (1–2), 305–316.
Borisova, A.Y., Pichavant, M., Polvé, M., Wiedenbeck, M., Freydier, R., Candaudap, F., 2006. Trace element geochemistry of the 1991Mt. Pinatubo silicicmelts, Philippines: implications for ore-forming potential of adakitic magmatism. Geochim. Cosmochim. Acta 70, 3702–3716.
Bourdon, E., Eissen, J.P., Monzier, M., Robin, C., Martin, H., 2002. Adakite-like lavas from Antisana volcano (Ecuador): Evidence from slab melt metasomatism beneath the Andean Northern volcanic zone. J. Petrol. 43, 99–217.
Bouzari, F., Hart, C.J.R., Bissig, T., Barker, S., 2016. Hydrothermal alteration revealed by apatite luminescence and chemistry: A potential indicator mineral for exploring covered porphyry copper deposits. Econ. Geol. 111, 1397–1410.
Boyce, J.W., Hervig, R.L., 2009. Apatite as a monitor of late–stage magmatic processes at Volcán Irazú, Costa Rica. Contrib. Mineral. Petrol. 157, 135–145.
Bruand, E., Storey, C., Fowler, M., 2014. Accessory mineral chemistry of high Ba–Sr granites from northern Scotland: Constraints on petrogenesis and records of whole–rock signature. J. Petrol. 55 (8), 1619–1651.
Candela, P.A., Holland, H.D., 1986. A mass transfer model for copper and molybdenum in magmatic hydrothermal systems; the origin of porphyry-type ore deposits. Econ. Geol. 81, 1–19.
Castillo, P.R., Janney, P.E., Solidum, R., 1999. Petrology and geochemistry of Camiguin Island, southern Philippines: Insights into the source of adakite and other lavas in a complex arc tectonic setting. Contrib. Miner. Petrol. 134, 33–51.
Castillo, P.R., 2012. Adakite petrogenesis. Lithos 134–135, 304–316.
Chauvel, C., Lewin, E., Carpentier, M., Carpentier, M., Arndt, N.T., Marini, J.C., 2008. Role of recycled oceanic basalt and sediment in generating the Hf–Nd mantle array. Nature Geoence 1 (1), 64–67.
Chang, Y.F., Liu, X.P., Wu, Y.C., 1991. The Copper-iron Belt of the Middle and Lower Reaches of the Changjiang River. Geological Publishing House, Beijing, pp. 1–379.
Chen, C.J., Chen, B., Li, Z., Wang, Z.Q., 2016a. Important role of magma mixing in generating the Mesozoic monzodioritic- granodioritic intrusions related to Cu mineralization, Tongling, East China: Evidence from petrological and in situ Sr-Hf isotopic data. Lithos 248–251, 80–93.
Chu, M.F., Wang, K.L., Griffin, W.L., Chung, S.L., O'Reilly, S.Y., Pearson, N.J., Iizuka, Y., 2009. Apatite composition: Tracing petrogenetic processes in Transhimalayan granitoids. J. Petrol. 50, 1829–1855.
Cui, B., Zhang, Z.Y., Zhao, L., 2002. Genetic mineralogy of garnets from the Tongguanshan copper deposit. Geol. Rev. 48, 275–278 (in Chinese with English abstract).
Defant, M.J., Drummond, M.S., 1990. Derivation of some modern arc magmas by melting of young subducted lithosphere. Nature 347, 662–665.
Defant, M.J., Kepezhinskas, P., 2001. Evidence suggests slab melting in arc magmas. EOS (Transactions, American Geophysical Union) 82, 65–69.
Deng, J.H., Yang, X.Y., Li, S., Gu, H.L., Mastoi, A.S., Sun, W.D., 2016. Partial melting of subducted paleo-Pacific plate during the early Cretaceous: Constraint from adakitic rocks in the Shaxi porphyry Cu-Au deposit, Lower Yangtze River Belt. Lithos 262, 651–667.
Deng, J.H., Yang, X.Y., Qi, H.S., Zhang, Z.F., Mastoi, A.S., Berador, A.E.G., Sun, W.D., 2019. Early cretaceous adakite from the atlas porphyry Cu-Au deposit in Cebu Island, Central Philippines: Partial melting of subducted oceanic crust. Ore Geol. Rev. 110, 102937.
Deng, J.H., Yang, X.Y., Zhang, L.P., Duan, L.A., Mastoi, A.S., Liu, H., 2020. An overview on the origin of adakites/adakitic rocks and related porphyry Cu-Au mineralization. Ore Geol. Rev. https://doi.org/10.1016/j.oregeorev.2020.103610.
Ding, T., Ma, D.S., Lu, J.J., Zhang, R.Q., 2015. Apatite in granitoids related to polymetallic mineral deposits in southeastern Hunan province, Shi-Hang zone, China: Implications for petrogenesis and metallogenesis. Ore Geol. Rev. 69, 104–117.
Dingwell, D.B., Hess, K.U., Romano, C., 1998. Extremely fluid behavior of hydrous peralkaline rhyolites. Earth Planet. Sci. Lett. 158, 31–38.
Drummond, M.S., Defant, M.J., 1990. A model for trondhjemite–tonalite–dacite genesis and crustal growth via slab melting: Archaean to modern comparisons. J. Geophys. Res. 95, 21503–21521.
Du, J.G., Du, Y.S., Cao, Y., 2018. Important role of hornblende fractionation in generating the adakitic magmas in Tongling, Eastern China: Evidence from amphibole megacryst and cumulate xenoliths and host gabbros. Int. Geol. Rev. https://doi.org/10.1080/00206814.2017.1418683.
Duan, X.X., Chen, B., Sun, K.K., Wang, Z.Q., Yan, X., Zhang, Z., 2019. Accessory mineral chemistry as a monitor of petrogenetic and metallogenetic processes: A comparative study of zircon and apatite from Wushan Cu- and Zhuxiling W(Mo)-mineralization-related granitoids. Ore Geol. Rev. 111, 102940.
Elliott, T., Plank, T., Zindler, A., White, W., Bourdon, B., 1997. Element transport from

slab to volcanic front at the Mariana arc. J. Geophys. Res. 102, 14991–15019.
Ewart, A., Griffin, W.L., 1994. Application of protonmicroprobe data to trace-element partitioning in volcanicrocks. Chem. Geol. 117, 251–284.
Filiberto, J., Treiman, A.H., 2009. The effect of chlorine on the liquidus of basalt: First results and implications for basalt genesis on Mars and Earth. Chem. Geol. 263, 60–68.
Foley, S., Tiepolo, M., Vannucci, R., 2002. Growth of early continental crust controlled by melting of amphibolite in subduction zones. Nature 417, 837–840.
Gagnevin, D., Daly, J.S., Kronz, A., 2010. Zircon texture and chemical composition as a guide to magmatic processes and mixing in a granitic environment and coeval volcanic system. Contrib. Mineral. Petrol. 159, 579–596.
Gammons, C.H., Williams-Jones, A.E., 1997. Chemical mobility of gold in the porphyry-epithermal environment. Econ. Geol. 92, 45–59.
Gibert, F., Pascal, M.-L., Pichavant, M., 1998. Gold solubility and speciation in hydrothermal solutions: Experimental study of the stability of hydrosulphide complex of gold (AuHS) at 350 to 450 C and 500 bars. Geochim. Cosmochim. Acta 62, 2931–2947.
Goss, A.R., Kay, S.M., 2009. Extreme high field strength element (HFSE) depletion and near-chondritic Nb/Ta ratios in Central Andean adakite-like lavas (~ 28°S, ~ 68°W). Earth Planet. Sci. Lett. 279, 97–109.
Green, T.H., Pearson, N.J., 1987. An experimental study of Nb and Ta partitioning between Ti-rich minerals and silicate liquids at high pressure and temperature. Geochim. Cosmochim. Acta 51, 55–62.
Gu, H.L., Yang, X.Y., Deng, J.H., Duan, L.A., Chen, L.J., 2020. Geochemical study of the Tonglingpo intrusion in the Guichi region: Significances of Cu-Au ore-forming. Acta Petrologica Sinica 36, 205–224 (in Chinese with English Abstract).
Guo, F., Fan, W., Wang, Y., Zhang, M., 2004. Origin of early Cretaceous calc-alkaline lamprophyres from the Sulu orogen in eastern China: Implications for enrichment processes beneath continental collisional belt. Lithos 78, 291–305.
Guo, J.L., Gao, S., Wu, Y.B., Li, M., Chen, K., Hu, Z.C., Liang, Z.W., Liu, Y.S., Zhou, L., Zong, K.Q., Zhang, W., Chen, H.H., 2014. 3.45 Ga granitic gneisses from the Yangtze Craton, South China: Implications for Early Archean crustal growth. Precambr. Res. 242, 82–95.
Guo, Z.F., Wilson, M., Liu, J.Q., 2007. Post-collisional adakites in south Tibet: Products of partial melting of subduction-modified lower crust. Lithos 96, 205–224.
Harlov, D.E., 2015. Apatite: A fingerprint for metasomatic processes. Elements 11, 171–176.
Hawkesworth, C.J., Kemp, A.I.S., 2006. Evolution of the continental crust. Nature 443, 811–817.
He, Y., Li, S., Hoefs, J., Huang, F., Liu, S.-A., Hou, Z., 2011. Post-collisional granitoids from the Dabie orogen: New evidence for partial melting of a thickened continental crust. Geochim. Cosmochim. Acta 75, 3815–3838.
Hedenquist, J.W., Lowenstern, J.B., 1994. The role of magmas in the formation of hydrothermal ore deposits. Nature 370, 519–527.
Hernández-Uribe, D., Hernández-Montenegro, J.D., Cone, K.A., Palin, R.M., 2020. Oceanic slab-top melting during subduction: Implications for trace-element recycling and adakite petrogenesis. Geology 48, 216–220.
Hezarkhani, A., Williams-Jones, A.E., Gammons, C.H., 1999. Factors controlling copper solubility and chalcopyrite deposition in the Sungun porphyry copper deposit. Iran. Mineralium Deposita 34, 770–783.
Hoefs, J., 2009. Stable Isotope Geochemistry, 6th Edition. Springer Verlag, Berlin Heidelberg. 285 pp.Hofmann, A.W., Jochum, K.P., Seufert, M., White, W.M., 1986. Nb and Pb in oceanic basalts: New constraints on mantle evolution. Earth and Planetary Science Letters 79, 33–45.
Hofmann, A., Jochum, K., Seufert, M., White, W., 1986. Nb and Pb in oceanic basalts: New constraints on mantle evolution. Earth Planet. Sci. Lett. 79, 33–45.
Hofmann, A.W., 2003. Sampling mantle heterogeneity through oceanic basalts: Isotopes and trace elements. Treatise Geochem. 2, 1–44.
Hoskin, P.W.O., Ireland, T.R., 2000. Rare earth element chemistry of zircon and its use as a provenance indicator. Geology 28, 627–630.
Hoskin, P.W.O., Schaltegger, U., 2003. The composition of zircon and igneous and metamorphic petrogenesis. Rev. Miner. Geochem. 53, 27–62.
Hou, Z.Q., Gao, Y.F., Qu, X.M., Rui, Z.Y., Mo, X.X., 2004. Origin of adakitic intrusives generated during mid-Miocene east-west extension in southern Tibet. Earth Planet Sci. Lett. 220, 139–155.
Hu, J., Liu, X.C., Chen, L.Y., Qu, W., Li, H.K., Geng, J.Z., 2013. A ~2.5 Ga magmatic event at the northern margin of the Yangtze craton: Evidence from U-Pb dating and Hf isotope analysis of zircons from the Douling Complex in the South Qinling orogen. Chin. Sci. Bull. 58, 3564–3579.
Hu, Z.L., Yang, X.Y., Duan, L.A., 2018. Geochemical study of Cretaceous magmatic rocks in Chuzhou region, low Yangtze River Metallogenic Belt : Implications for petrogenesis and Cu-Au mineralization. Int. Geol. Rev. https://doi.org/10.1080/00206814.2017.1373606.
Jahn, B.M., Wu, F.Y., Lo, C.H., Tsai, C.H., 1999. Crust–mantle interaction induced by deep subduction of the continental crust: geochemical and Sr–Nd isotopic evidence from post-collisional mafic–ultramafic intrusions of the northern Dabie complex, central China. Chem. Geol. 157, 119–146.
Jiang, X.Y., Li, H., Ding, X., Wu, K., Guo, J., Liu, J.Q., Sun, W.D., 2018a. Formation of A-Type granites in the Lower Yangtze River Belt: A perspective from apatite geochemistry. Lithos 304–307, 125–134.
Jiang, X.Y., Ling, M.X., Wu, K., Zhang, Z.K., Sui, Q.L., Sun, W.D., Xia, X.P., 2018b. Insights into the origin of coexisting A1– And A2–Type granites: Implications from zircon Hf–O isotopes of the Huayuangong intrusion in the Lower Yangtze River Belt, eastern China. Lithos 318–319, 230–243.
Kawamotoa, T., Yoshikawa, M., Kumagai, Y., Mirabueno, M.H.T., Okuno, M., 2013. Mantle wedge infiltrated with saline fluids from dehydration and decarbonation of subducting slab. PNAS 110, 9663–9668.
Kelley, K.A., Plank, T., Farr, L., Ludden, J., Staudigel, H., 2005. Subduction cycling of U, Th, and Pb. Earth Planet. Sci. Lett. 234, 369–383.
Kemp, A.I.S., Hawkesworth, C.J., Foster, G.L., Paterson, B.A., Woodhead, J.D., Hergt, J.M., Gray, C.M., Whitehouse, M.J., 2007. Magmatic and crustal differentiation history of granitic rocks from Hf–O isotopes in zircon. Science 16, 980–983.
Kempton, P.D., Harmon, R.S., 1992. Oxygen isotope evidence for large-scale hybridization of the lower crust during magmatic underplating. Geochim. Cosmochim. Acta 56, 971–986.
Kendrick, M.A., Scambelluri, M., Honda, M., Phillips, D., 2011. High abundances of noble gas and chlorine delivered to the mantle by serpentinite subduction. Nat. Geosci. 4, 807–812.
Kepezhinskas, P., McDermott, F., Defant, M.J., Hochstaedter, A., Drummond, M.S., Hawkesworth, C.J., Koloskov, A., Maury, R.C., Bellon, H., 1997. Trace element and Sr-Nd-Pb isotopic constraints on a three-component model of Kamchatka Arc petrogenesis. Geochim. Cosmochim. Acta 61, 577–600.
König, S., Schuth, S., 2011. Deep melting of old subducted oceanic crust recorded by superchondritic Nb/Ta in modern island arc lavas. Earth Planet. Sci. Lett. 301, 265–274.
Kusebauch, C., John, T., Whitehouse, M.J., Klemme, S., Putnis, A., 2015. Distribution of halogens between fluid and apatite during fluid–mediated replacement processes. Geochim. Cosmochim. Acta 170, 225–246.
Lassiter, J.C., Hauri, E.H., Nikogosian, I.K., Barsczus, H.G., 2002. Chlorine–potassium variations in melt inclusions from Raivavae and Rapa, Austral Islands: constraints on chlorine recycling in the mantle and evidence for brine-induced melting of oceanic crust. Earth Planet. Sci. Lett. 202, 525–540.
Li, J.W., Zhao, X.F., Zhou, M.F., Ma, C.Q., Sergio De Souza, Z., Vasconcelos, P., 2009a. Late Mesozoic magmatism from the Daye region, eastern China: U-Pb ages, petrogenesis, and geodynamic implications. Contrib. Miner. Petrol. 157, 383–409.
Li, N.B., Niu, H.C., Yang, W.B., Lai, C.K., Zhao, Z.H., 2019. Orogenic root delamination induced by eclogitization of thickened lower crust in the Chinese Western Tianshan: Constraints from adakites. J. Geophys. Res. Solid Earth 124, 11089–11104. https://doi.org/10.1029/2019JB018354.
Li, X.H., Liu, Y., Li, Q.L., Guo, C.H., Chamberlain, K.R., 2009b. Precise determination of Phanerozoic zircon Pb/Pb age by multicollector SIMS without external standardization. Geochem. Geophys. Geosyst. 10, Q04010.
Li, X.H., Liu, D.Y., Sun, M., Li, W.X., Liang, X.R., Liu, Y., 2004. Precise Sm–Nd and U-Pb isotopic dating of the super-giant Shizhuyuan polymetallic deposit and its host granite, Southeast China. Geol. Mag. 141, 225–231.
Li, X.H., Li, W.X., Li, Q.L., Wang, X.C., Liu, Y., Yang, Y.H., 2010a. Petrogenesis and tectonic significance of the ~850 Ma Gangbian alkaline complex in South China: evidence from in situ zircon U-Pb dating, Hf–O isotopes and whole-rock geochemistry. Lithos 114, 1–15.
Li, X.H., Long, W.G., Li, Q.L., 2010b. Penglai zircon megacrysts: a potential new working reference material for microbeam determination of Hf–O isotopes and U-Pb age. Geostand. Geoanal. Res. 34, 117–134.
Li, X.H., Tang, G.Q., Gong, B., Yang, Y.H., Hou, K.J., Hu, Z.C., Li, Q.L., Liu, Y., Li, W.X., 2013. Qinghu zircon: A working reference for microbeam analysis of U-Pb age and Hf and O isotopes. Chin. Sci. Bull. 58, 4647–4654.
Li, S., Yang, X.Y., Yu, H., Sun, W.D., 2014. Petrogenesis and mineralization of the Fenghuangshan skarn Cu-Au deposit, Tongling ore cluster field, Lower Yangtze metallogenic belt. Ore Geology Reriews 58, 148–162.
Ling, M.X., Wang, F.Y., Ding, X., Hu, Y.H., Zhou, J.B., Zartman, R.E., Yang, X.Y., Sun, W.D., 2009. Cretaceous ridge subduction along the lower yangtse River Belt, Eastern China. Econ. Geol. 104, 303–321.
Ling, M.X., Wang, F.Y., Ding, X., Zhou, J.B., Sun, W.D., 2011. Different origins of adakites from the Dabie Mountains and the Lower Yangtze River belt in eastern China: Geochemical constraints. Int. Geol. Rev. 53, 727–740. https://doi.org/10.1080/00206814.2010.482349.
Liu, S.A., Li, S.G., He, Y.S., Huang, F., 2010. Geochemical contrasts between early Cretaceous ore-bearing and orebarren high-Mg adakites in central-eastern China: Implications for petrogenesis and Cu-Au mineralization. Geochim. Cosmochim. Acta 74, 7160–7178. https://doi.org/10.1016/j.gca.2010.09.003.
Liu, Y.S., Hu, Z.C., Gao, S., Gunther, D., Xu, J., Gao, C.G., Chen, H.H., 2008. In situ analysis of major and trace elements of anhydrous minerals by LA-ICP-MS without applying an internal standard. Chem. Geol. 257, 34–43.
Ludwig, K.R., 2008. Users' manual for Isoplot 3.70: a geochronological toolkit for Mircrosoft Excel. Berkeley Geochronology Center Special Publication No. 4. Berkeley, California.
Luo, Z.B., Xue, S., Zhang, L.P., Li, H., Li, C.Y., Zhang, H., Liu, Y.L., Ling, M.X., Sun, W.D., 2018. Origin of Early Cretaceous Guandian adakitic pluton in central eastern China: Partial melting of delaminated lower continental crust triggered by ridge subduction. Int. Geol. Rev. 60, 1707–1720.
Ma, Q., Zheng, J.P., Xu, Y.G., Griffin, W.L., Zhang, R.S., 2015. Are continental "adakites" derived from thickened or foundered lower crust? Earth Planet. Sci. Lett. 419, 125–133.
Mahoney, J.J., Frei, R., Tejada, M.L.G., Mo, X.X., Leat, P.T., 1998. Tracing the Indian ocean mantle domain through time: Isotopic results from old west Indian, east Tethyan and south Pacific seafloor. J. Petrol. 39, 1285–1306.
Mao, J.W., Wang, Y.T., Lehmann, B., Yu, J.J., Du, A.D., Mei, Y.X., Li, Y.F., Zang, W.S., Stein, H.J., Zhou, T.F., 2006. Molybdenite Re-Os and albite $^{40}Ar/^{39}Ar$ dating of Cu-Au- Mo and magnetite porphyry systems in the Yangtze River valley and metallogenic implications. Ore Geol. Rev. 29, 307–324.
Mao, J.W., Xie, G.Q., Duan, C., Pirajno, F., Ishiyama, D., Chen, Y.C., 2011. A tectonogenetic model for porphyryskarn- stratabound Cu-Au-Mo-Fe and magnetite-apatite deposits along the Middle-Lower Yangtze River valley, Eastern China. Ore Geol. Rev.

43, 294–314.
Mao, M., Rukhlov, A.S., Rowins, S.M., Spence, J., Coogan, L.A., 2016. Apatite trace Element compositions: a robust new tool for mineral exploration. Econ. Geol. 111, 1187–1222.
Mathez, E.A., Webster, J.D., 2005. Partitioning behavior of chlorine and fluorine in the system apatite-silicate melt-fluid. Geochim. Cosmochim. Acta 69, 1275–1286.
Martin, H., 1999. The adakitic magmas: modern analogues of Archaean granitoids. Lithos 46 (3), 411–429.
Martin, H., Smithies, R., Rapp, R., Moyen, J.F., Champion, D., 2005. An overview of adakite, tonalite–trondhjemite– granodiorite (TTG), and sanukitoid: Relationships and some implications for crustal evolution. Lithos 79, 1–24.
McCulloch, M.T., Gamble, A.J., 1991. Geochemical and geodynamical constraints on subduction zone magmatism. Earth Planet. Sci. Lett. 102, 358–374.
McDonough, W.F., Sun, S.S., 1995. The composition of the earth. Chem. Geol. 120, 223–253.
Miles, A.J., Graham, C.M., Hawkesworth, C.J., Gillespie, M.R., Hinton, R.W., 2013. Evidence for distinct stages of magma history recorded by the compositions of accessory apatite and zircon. Contrib. Mineral. Petrol. 166 (1), 1–19.
Miles, A.J., Graham, C.M., Hawkesworth, C.J., Gillespie, M.R., Hinton, R.W., Bromiley, G.D., 2014. Apatite: a new redox proxy for silicic magmas? Geochim. Cosmochim. Acta 132, 101–119.
Moyen, J.F., 2009. High Sr/Y and La/Yb ratios: The meaning of the “adakitic signature”. Lithos 112, 556–574.
Moyen, J.F., Martin, H., 2012. Forty years of TTG research. Lithos 148, 312–336. https://doi.org/10.1016/j.lithos.2012.06.010.
Muehlenbachs, K., 1998. The oxygen isotopic composition of the oceans, sediments and the seafloor. Chem. Geol. 145, 263–273.
Mungall, J.E., 2002. Roasting the mantle: Slab melting and the genesis of major au and au-rich cu deposits. Geology 30, 915–918.
Nadeau, O., Willians-Jones, A.E., Stix, J., 2010. Sulphide magma as a source of metals in arcrelated magmatic hydrothermal ore fluids. Nat. Geosci. 3, 501–505.
Nasdala, L., Hofmeister, W., Norberg, N., Mattinson, J.M., Corfu, F., Dörr, W., Kamo, S.L., Kennedy, A.K., Kronz, A., Reiners, P.W., Frei, D., Kosler, J., Wan, Y., Götze, J., Häger, T., Kröner, A., Valley, J.W., 2008. Zircon M257 – A homogeneous natural reference material for the ion microprobe U-Pb analysis of zircon. Geostand. Geoanal. Res. 32, 47–265.
Noll, P.D., Newsom, H.E., Leeman, W.P., Ryan, J.G., 1996. The role of hydrothermal fluids in the production of subduction zone magmas: Evidence from siderophile and chalcophile trace elements and boron. Geochim. Cosmochim. Acta 60, 587–611.
Oyarzún, R., Márquez, A., Lillo, J., López, I., Rivera, S., 2001. Giant vs small porphyry copper deposits of Cenozoic age in northern Chile: Adakitic vs normal calc-alkaline magmatism. Miner. Deposita 36, 794–798.
Pan, L.C., Hu, R.Z., Wang, X.S., Bi, X.W., Zhu, J.J., Li, C.S., 2016. Apatite trace element and halogen compositions as petrogenetic-metallogenic indicators: Examples from four granite plutons in the Sanjiang region, SW China. Lithos 254–255, 118–130.
Pan, Y.M., Dong, P., 1999. The lower Changjiang (Yangzi/ Yangtze River) metallogenic belt, east central China: Intrusion- and wall rock-hosted Cu-Fe-Au, Mo, Zn, Pb, Ag deposits. Ore Geol. Rev. 15, 177–242.
Patiño Douce, A.E.P., Roden, M.F., Chaumba, J., Fleisher, C., Yogodzinski, G., 2011. Compositional variability of terrestrial mantle apatites, thermodynamic modeling of apatite volatile contents, and the halogen and water budgets of planetary mantles. Chem. Geol. 288, 14–31.
Petford, N., Atherton, M., 1996. Na-rich partial melts from newly underplated basaltic crust: The Cordillera Blanca Batholith, Peru. J. Petrol. 37, 1491–1521.
Plank, T., Langmuir, C., 1998. The chemical composition of subducting sediment and its consequences for the crust and mantle. Chem. Geol. 145, 325–394.
Prowatke, S., Klemme, S., 2005. Effect of melt composition on the partitioning of trace elements between titanite and silicate melt. Geochim. Cosmochim. Acta 69, 695–709.
Qian, L., Wang, Y., Xie, J.C., Sun, W.D., 2019. The Late Mesozoic granodiorite and polymetallic mineralization in southern Anhui Province, China: A perspective from apatite geochemistry. Solid Earth Sci. 4, 178–189.
Qin, X.L., Du, Y.S., Lee, H.K., Yin, J.W., Guo, X.F., 2003. Fe-Ti oxide and Fe-Cu sulfide exsolution in amphibole cumulate xenoliths from granodiorite in Tongling, Anhui Province. Chin. Sci. Bull. 48, 2626–2634.
Rapp, R.P., Watson, E.B., Miller, C.F., 1991. Partial melting of amphibolite/eclogite and the origin of Archean trondhjemites and tonalites. Precambr. Res. 51, 1–25.
Rapp, R.P., Watson, E.B., 1995. Dehydration melting of metabasalt at 8–32 kbar: Implications for continental growth and crust-mantle recycling. J. Petrol. 36, 891.
Reynard, B., 2013. Serpentine in active subduction zones. Lithos 178, 171–185.
Richards, J.P., Kerrich, R., 2007. Special paper: Adakite-like rocks: their diverse origins and questionable role in metallogenesis. Econ. Geol. 102, 537–576.
Rudnick, R.L., Gao, S., 2003. Composition of the continental crust. Treat. Geochem. 3, 1–64.
Rudnick, R.L., Gao, S., 2014. Composition of the Continental Crust. Treatise Geochem. 3, 1–51.
Sha, L.K., Chappell, B.W., 1999. Apatite chemical composition, determined by electron microprobe and laser-ablation inductively coupled plasma mass spectrometry, as a probe into granite petrogenesis. Geochim. Cosmochim. Acta 63, 3861–3881.
J.G. Shellnutt J. Dostal Derivation of the Early Carboniferous Wedgeport pluton by crystal fractionation of a mafic parental magma: A rare case of an A-type granite within the Meguma terrane (Nova Scotia 2019 Geological Magazine Canada) 10.1017/S0016756819000694.
Shimoda, G., Tatsumi, Y., Nohda, S., Ishizaka, K., Jahn, B.M., 1998. Setouchi high-Mg andesites revisited: geochemical evidence for melting of subducting sediments. Earth Planet. Sci. Lett. 160, 479–492.
Shimoda, G., Tatsumi, Y., 1999. Generation of rhyolite magmas by melting of subducting sediments in Shodo-Shima island, Southwest Japan, and its bearing on the origin of high-Mg andesites. Isl. Arc 8, 383–392.
Shimoda, G., Tatsumi, Y., Morishita, Y., 2003. Behavior of subducting sediments beneath an arc under a high geothermal gradient: Constraints from the Miocene SW Japan arc. Geochem. J. 37, 503–518.
Shimoda, G., 2009. Genetic link between EMI and EMII: An adakite connection. Lithos 112, 591–602.
Sillitoe, R.H., 2010. Porphyry copper systems. Econ. Geol. 105, 3–41.
Sisson, T.W., 1994. Hornblende-melt trace-element partitioning measured by ion microprobe. Chem. Geol. 117, 331–344.
Sláma, J., Košler, J., Condon, D.J., Crowley, J.L., Gerdes, A., Hanchar, J.M., Horstwood, M.S.A., Morris, G.A., Nasdala, L., Norberg, N., Schaltegger, U., Schoene, B., Tubrett, M.N., Whitehouse, M.J., 2008. Plešovice zircon – A new natural reference material for U-Pb and Hf isotopic microanalysis. Chem. Geol. 249, 1–35.
Stroncik, N.A., Haase, K.M., 2004. Chlorine in oceanic intraplate basalts: Constraints on mantle sources and recycling processes. Geology 32, 945–948.
Sun, S.S., McDonough, W.F., 1989. Chemical and isotopic systematics of oceanic basalts: Implications for mantle composition and processes. Geol. Soc.: London, UK 42, 313–345.
Sun, W.D., Xie, Z., Chen, J.F., Zhang, X., Chai, Z.F., Du, A.D., Zhao, J.S., Zhang, C.H., Zhou, T.F., 2003. Os-Os dating of copper and molybdenum deposits along the middle and lower reaches of the Yangtze River, China. Econ. Geol. Bull. Soc. Econ. Geol. 98, 175–180.
Sun, W.D., Arculus, R.J., Kamenetsky, V.S., Binns, R.A., 2004. Release of gold-bearing fluids in convergent margin magmas prompted by magnetite crystallization. Nature 431, 975–978.
Sun, W.D., Hu, Y.H., Kamenetsky, V.S., Eggins, S.M., Chen, M., Arculus, R.J., 2008. Constancy of Nb/U in the mantle revisited. Geochim. Cosmochim. Acta 72, 3542–3549.
Sun, W.D., Ling, M.X., Chung, S.L., Ding, X., Yang, X., 2010a. Slab melting and its implications for copper ore mineralization and future exploration. Geochim. Cosmochim. Acta 74, A1007.
Sun, W.D., Ling, M.X., Yang, X.Y., Fan, W.M., Ding, X., Liang, H.Y., 2010b. Ridge subduction and porphyry copper-gold mineralization: An overview. Sci. China Earth Sci. 53, 475–484.
Sun, W.D., Zhang, H., Ling, M.X., Ding, X., Chung, S.L., Zhou, J.B., Yang, X.Y., Fan, W.M., 2011. The genetic association of adakites and Cu–Au ore deposits. Int. Geol. Rev. 53, 691–703.
Sun, W.D., Ling, M.X., Chung, S.L., Ding, X., Yang, X.Y., Liang, H.Y., Fan, W.M., Goldfarb, R., Yin, Q.Z., 2012. Geochemical constraints on adakites of different origins and copper mineralization. J. Geol. 120, 105–120.
Sun, W.D., Liang, H.Y., Ling, M.X., Zhan, M.Z., Ding, X., Zhang, H., Yang, X.Y., Li, Y.L., Ireland, T.R., Wei, Q.R., Fan, W.M., 2013. The link between reduced porphyry copper deposits and oxidized magmas. Geochim. Cosmochim. Acta 103, 263–275.
Sun, W.D., Huang, R.F., Li, H., Hu, Y.B., Zhang, C.C., Sun, S.J., Zhang, L.P., Ding, X., Li, C.Y., Zartman, R.E., Ling, M.X., 2015. Porphyry deposits and oxidized magmas. Ore Geol. Rev. 65, 97–131.
Sun, W.D., Li, C.Y., Hao, X.L., Ling, M.X., Ireland, T., Ding, X., Fan, W.M., 2016. Oceanic anoxic events, subduction style and molybdenum mineralization. Solid Earth Sci. 1, 64–73.
Sun, W.D., Wang, J.T., Zhang, L.P., Zhang, C.C., Li, H., Ling, M.X., Ding, X., Li, C.Y., Liang, H.Y., 2017. The formation of porphyry copper deposits. Acta Geochimica 36, 9–15.
Tanaka, T., Togashi, S., Kamioka, H., Amakawa, H., Kagami, H., Hamamoto, T., Yuhara, M., Orihashi, Y., Yoneda, S., Shimizu, H., Kunimaru, T., Takahashi, K., Yanagi, T., Nakano, T., Fujimaki, H., Shinjo, R., Asahara, Y., Tanimizu, M., Dragusanu, C., 2000. JNdi–1: A neodymium isotopic reference in consistency with LaJolla neodymium. Chem. Geol. 168, 279–281.
Tatsumi, Y., 1986. Chemical characteristics of £uid phase released from a subduction lithosphere and origin of arc magma: Evidence from high-pressure experiments and natural rocks. J. Volcanol. Geotherm. Res. 29, 293–309.
Taylor, S.R., McLennan, S.M., 1995. The geochemical evolution of the continental crust. Rev. Geophys. 33, 241–265.
Thiéblemont, D., Stein, G., Lescuyer, J.L., 1997. Epithermal and porphyry deposits: The adakite connection. Comptes Rendus de l'Académie des Sci. Paris 325, 103–109.
Tian, S.H., Ding, T.P., Hou, Z.Q., Yang, Z.S., Xie, Y.L., Wang, Y.B., Wang, X.C., 2005. REE and stable isotope geochemistry of the Xiaotongguanshan copper deposit, Tongling, Anhui. Geol. China 32, 604–613.
Valley, J.W., Lackey, J.S., Cavosie, A.J., Clechenko, C.C., Spicuzza, M.J., Basei, M.A.S., Bindeman, I.N., Ferreira, V.P., Sial, A.N., King, E.M., Peck, W.H., Sinha, A.K., Wei, C.S., 2005. 4.4 billion years of crustal maturation: Oxygen isotope ratios of magmatic zircon. Contrib. Miner. Petrol. 150, 561–580.
Wang, F.Y., Liu, S.A., Li, S.G., He, Y.S., 2013a. Constrasting zircon Hf-O isotopes and trace elements between ore-bearing and ore-barren adakitic rocks in central-eastern China: Implications for genetic relation to Cu-Au mineralization. Lithos 156–159, 97–111.
Wang, H., Zhao, Z., Yang, X.Y., Gu, H.L., Zheng, Y., Nguyen, T.A., 2020. Genesis of the Baoshujian Cu-polymetal deposit in Anqing-Guichi ore-cluster area: Constraints from petrogeochemistry and geochronology. Acta Petrologica Sinica 36, 184–204 (in Chinese with English abstract).
Wang, J.Z., Li, J.W., Zhao, X.F., Qian, Z.Z., Ma, C.Q., 2008. Genesis of the Chaoshan gold deposit and its host intrusion, Tongling area: Constraints from $^{40}Ar/^{39}Ar$ ages and elemental and Sr-Nd-O-C-S isotope geochemistry. Acta Petrologica Sinica 24, 1875–1888 (in Chinese with English abstract).
Wang, Q., Xu, J.F., Zhao, Z.H., Xiong, X.L., Bao, Z.W., 2003. Petrogenesis of the Mesozoic intrusive rocks in the Tongling area. Anhui Province, China and their constraint on geodynamic process: Science in China Series D: Earth Sciences 46, 801–815.

Wang, Q., Xu, J.F., Zhao, Z.H., Bao, Z.W., Xu, W., Xiong, X.L., 2004. Cretaceous high-potassium intrusive rocks in the Yueshan-Hongzhen area of east China: Adakites in an extensional tectonic regime within a continent. Geochem. J. 38, 417–434.
Wang, Q., Wyman, D.A., Xu, J.F., Zhao, Z.H., Jian, P., Xiong, X.L., Bao, Z.W., Li, C.F., Bai, Z.H., 2006. Petrogenesis of Cretaceous adakitic and shoshonitic igneous rocks in the Luzong area, Anhui Province (eastern China): Implications for geodynamics and Cu-Au mineralization. Lithos 89, 424–446.
Wang, Q., Wyman, D.A., Xu, J.F., Zhao, Z.H., Jian, P., Zi, F., 2007. Partial melting of thickened or delaminated lower crust in the middle of Eastern China: Implications for Cu-Au mineralization. J. Geol. 115, 149–161.
Wang, S.W., Zhou, T.F., Yuan, F., Fan, Y., Cooke, D.R., Zhang, L.J., Fu, B., White, N.C., 2016. Geochemical characteristics of the Shujiadian Cu deposit related intrusion in Tongling: Petrogenesis and implications for the formation of porphyry Cu systems in the Middle-Lower Yangtze River valley metallogenic belt, eastern China. Lithos 252–253, 185–199.
Wang, X.L., Zhou, J.C., Wan, Y.S., Kitajim, K., Wang, D., Bonamici, C., Qiu, J.S., Sun, T., 2013b. Magmatic evolution and crustal recycling for Neoproterozoic strongly peraluminous granitoids from southern China: Hf and O isotopes in zircon. Earth Planet. Sci. Lett. 366, 71–82.
Workman, R.K., Hart, S.R., 2005. Major and trace element composition of the depleted MORB mantle (DMM). Earth Planetary Sci. Lett. 231, 53–72.
Wu, C.L., Wang, Z.H., Qiao, D.W., Li, H.B., Hao, M.Y., Shi, R.D., 2000. Types of enclaves and their features and origins in intermediate-acid intrusive rocks from the Tongling district, Anhui Province, China. Acta Geologica Sinica (English Edition) 74, 54–67.
Wu, C.L., Dong, S.W., Wu, D., Zhang, X., Ernst, W.G., 2017. Late Mesozoic high-K calc-alkaline magmatism in SE China: The Tongling example. Int. Geol. Rev.
Xie, J.C., Yang, X.Y., Sun, W.D., Du, J.U., 2012. Early Cretaceous dioritic rocks in the Tongling region, eastern China: implications for the tectonic settings. Lithos 150, 49–61.
Xie, J.C., Yang, X.Y., Sun, W.D., Du, J.G., Xu, W., Wu, L.B., Wang, K.Y., Du, X.W., 2009. Geochronological and geochemical constraints on formation of the Tongling metal deposits, middle Yangtze metallogenic belt, east-central China. Int. Geol. Rev. 51, 388–421.
Xie, J.C., Wang, Y., Li, Q.Z., Liu, J.M., Yan, J., Sun, W.D., 2017. Early Cretaceous adakitic rocks in the Anqing region, southeastern China: Constraints on petrogenesis and metallogenic significance. Int. Geol. Rev. https://doi.org/10.1080/00206814.2017.1362672.
Xie, J.C., Wang, Y., Li, Q.Z., Yan, J., Sun, W.D., 2018. Petrogenesis and metallogenic implications of Late Mesozoic intrusive rocks in the Tongling region, eastern China: A case study and perspective review. Int. Geol. Rev. 60, 1361–1380.
Xie, J.C., Tang, D.W., Xia, D.M., Wang, Y., Li, Q.Z., Yan, J., Yang, X.Y., Sun, W.D., 2019. Geochronological and geochemical constraints on the formation of Chizhou Cu-Mo polymetallic deposits, middle and lower Yangtze metallogenic belt, eastern China. Ore Geol. Rev. 109, 322–347.
Xiong, X.L., Adam, J., Green, T.H., 2005. Rutile stability and rutile/melt HFSE partitioning during partial melting of hydrous basalt: Implications for TTG genesis. Chem. Geol. 218, 339–359.
Xiong, X.L., Keppler, H., Audétat, A., Ni, H., Sun, W., Li, Y., 2011. Partitioning of Nb and Ta between rutile and felsic melt and the fractionation of Nb/Ta during partial melting of hydrous metabasalt. Geochim. Cosmochim. Acta 75, 1673–1692.
Xu, X.S., Fan, Q.C., O'Reilly, S.Y., Jiang, S.Y., Griffin, W.L., Wang, R.C., Qiu, J.S., 2004. U-Pb dating of zircons from quartz diorite and its enclaves at Tongguanshan in Anhui and its petrogenetic implication. Chin. Sci. Bull. 49, 2073–2082.
Xu, L., Xie, Q.Q., Zhou, Y.F., Chen, P., Sun, S.H., Chen, T.H., 2019. Mineralogical characteristics of colloform pyrite from Tongguanshan ore field and its implications for mineralization of the stratabound sulfide deposit in Tongling mineralization cluster, Anhui Province. Acta Petrologica Sinica 35, 3721–3733.
Yan, H.Y., Wang, F.Y., Gu, H.O., Sun, H., Ge, C., 2020. Geochemical and Sr-Nd-Pb-Hf isotopic characteristics of Muchen Pluton in Southeast China, Constrain the petrogenesis of alkaline A-type magma. Minerals 10, 80.
Yan, J., Chen, J.F., Xu, X.S., 2008. Geochemistry of Cretaceous mafic rocks from the Lower Yangtze region, eastern China: characteristics and evolution of the lithospheric mantle. J. Asian Earth Sci. 33, 177–193.
Yan, J., Liu, J.M., Li, Q.Z., Xing, G.F., Liu, X.Q., Xie, J.C., Chu, X.Q., Chen, Z.F., 2015. In situ zircon Hf-O isotopic analyses of late Mesozoic magmatic rocks in the Lower Yangtze River Belt, central eastern China: Implications for petrogenesis and geodynamic evolution. Lithos 227, 57–76.
Yang, X.Y., Yang, X.M., Zhang, Z.W., Chi, Y.Y., Yu, L.F., Zhang, Q.M., 2011. A porphyritic copper (gold) ore-forming model for the Shaxi-Changpushan district, Lower Yangtze metallogenic belt, China: Geological and geochemical constraints. Int. Geol. Rev. 53, 580–611.
Yang, Y.Z., Chen, F.K., Siebel, W., Zhang, H., Long, Q., He, J.F., Hou, Z.H., Zhu, X.Y., 2014. Age and composition of Cu-Au related rocks from the lower Yangtze River belt: Constraints on paleo-Pacific slab roll-back beneath eastern China. Lithos 202–203, 331–346.
Yuan, H.L., Gao, S., Dai, M.N., Zong, C.L., Günther, D., Fontaine, G.H., Liu, X.M., Diwu, C.R., 2008. Simultaneous determinations of U-Pb age, Hf isotopes and trace element compositions of zircon by excimer laser-ablation quadrupole and multiple-collector ICP-MS. Chem. Geol. 247, 100–118.
Zhai, Y.S., Yao, S.Z., Lin, X.D., Zhou, X.N., Wan, T.F., Jin, F.Q., Zhou, Z.G., 1992. Fe–Cu (Au) Metallogeny of the Middle-Lower Changjiang Region. Geological Publishing House, Beijing, v, pp. 235.
Zhai, Y.S., Xiong, Y.L., Yao, S.Z., Lin, X.D., 1996. Metallogeny of copper and iron deposits in the Eastern Yangtze Craton, east-central China. Ore Geol. Rev. 11, 229–248.
Zhang, B., Guo, F., Zhang, X., Wu, Y., Wang, G., Zhao, L., 2019a. Early Cretaceous subduction of Paleo-Pacific Ocean in the coastal region of SE China: Petrological and geochemical constraints from the mafic intrusions. Lithos 334, 8–24.
Zhang, C.C., Sun, W.D., Wang, J.T., Zhang, L.P., Sun, S.J., Wu, K., 2017. Oxygen fugacity and porphyry mineralization: A zircon perspective of Dexing porphyry Cu deposit, China. Geochim. Cosmochim. Acta 206, 343–363.
Zhang, L.P., Zhang, R.Q., Wu, K., Chen, Y.X., Li, C.Y., Hu, Y.B., He, J.J., Liang, J.L., Sun, W.D., 2018. Late Cretaceous granitic magmatism and mineralization in the Yingwuling W-Sn deposit, South China: Constraints from zircon and cassiterite U-Pb geochronology and wholerock geochemistry. Ore Geol. Rev. 96, 115–129.
Zhang, L.P., Zhang, R.Q., Chen, Y.X., Sun, S.J., Liang, J.L., Sun, W.D., 2019b. Geochronology and geochemistry of the Late Cretaceous Xinpeng granitic intrusion, South China: Implication for Sn-W mineralization. Ore Geol. Rev. 113, 103075.
Zhang, S.B., Zheng, Y.F., Wu, Y.B., Zhao, Z.F., Gao, S., Wu, F.Y., 2006. Zircon U-Pb age and Hf isotope evidence for 3.8 Ga crustal remnant and episodic reworking of Archean crust in South China. Earth Planet. Sci. Lett. 252, 56–71.
Zhang, S.B., Zheng, Y.F., 2013. Formation and evolution of Precambrian continental lithosphere in South China. Gondwana Res. 23, 1241–1260.
Zhao, C.C., Yang, X.Y., Feng, M., Sun, W.D., Hong, C.C., Sun, J., Hu, J.J., Tang, S.P., 2012. Mineralogical and geochemical characteristics of the Tongguanshan pluton and significance of magma crystallization kinetics. Acta Geol. Sin. 86, 1749–1760 (in Chinese with English abstract).
Zhu, X.Q., Wang, Z.G., Huang, Y., Wang, H.L., 2004. REE content and distribution in apatite and its geological tracing significance. Chinese Rare Earths 25, 41–45.